(2)

TITAN CORPORATION

OPTICAL TECHNIQUE FOR THE MEASUREMENT OF HIGH TEMPERATURE MATERIAL EROSION

FINAL REPORT

Excellence In All Endeavors

OPTICAL TECHNIQUE FOR THE MEASUREMENT OF HIGH TEMPERATURE MATERIAL EROSION

FINAL REPORT

AUGUST 1988

SDL NO. 88-2439-09/MA

K. A. ARUNKUMAR, C. FITZPATRICK AND M. AZZAZY

Prepared for:

AIR FORCE OFFICE OF SCIENTIFIC RESEARCH
Bolling Air Force Base
Washington, DC 20332

Under Contract: F49620-85-0046

SPECTRON
DEVELOPMENT
LABORATORIES, INC.

Unclassified
SECURITY CLASSIFICATION OF THIS PAGE

ADA205092

REPORT DOCUMENTATION PAGE

Form Approved
OMB No. 0704-0188

1a. REPORT SECURITY CLASSIFICATION: Unclassified	1b. RESTRICTIVE MARKINGS
2a. SECURITY CLASSIFICATION AUTHORITY	3. DISTRIBUTION/AVAILABILITY OF REPORT: Approved for public release; distribution is unlimited.
2b. DECLASSIFICATION/DOWNGRADING SCHEDULE	
4. PERFORMING ORGANIZATION REPORT NUMBER(S): 88-2439-09	5. MONITORING ORGANIZATION REPORT NUMBER(S): AFOSR-TR- 89-0231
6a. NAME OF PERFORMING ORGANIZATION: Spectron Development Laboratories; 6b. OFFICE SYMBOL (If applicable)	7a. NAME OF MONITORING ORGANIZATION: AFOSR/NA
6c. ADDRESS (City, State, and ZIP Code): 3535 Hyland Ave., Suite 102, Costa Mesa, CA 92626	7b. ADDRESS (City, State, and ZIP Code): Building 410, Bolling AFB DC 20332-6448
8a. NAME OF FUNDING/SPONSORING ORGANIZATION: AFOSR/NA; 8b. OFFICE SYMBOL (If applicable): NA	9. PROCUREMENT INSTRUMENT IDENTIFICATION NUMBER: F49620-85-C-0046
8c. ADDRESS (City, State, and ZIP Code): Building 410, Bolling AFB DC 20332-6448	10. SOURCE OF FUNDING NUMBERS: PROGRAM ELEMENT NO. 61102F; PROJECT NO. 2308; TASK NO. A3; WORK UNIT ACCESSION NO.

11. TITLE (Include Security Classification)
(U) Optical Technique for the Measurement of High Temperature Material Erosion

12. PERSONAL AUTHOR(S)
K. A. Arunkumar, C, Fitzpatrick and M. Azzazy

13a. TYPE OF REPORT	13b. TIME COVERED	14. DATE OF REPORT (Year, Month, Day)	15. PAGE COUNT
Final Report	FROM 3/1/85 TO 8/31/88	1988 August 30	43

16. SUPPLEMENTARY NOTATION

17. COSATI CODES		
FIELD	GROUP	SUB-GROUP

18. SUBJECT TERMS (Continue on reverse if necessary and identify by block number)
Common Path Interferometer, Profilometry, Coaxial Birefringent Ray (COBRA) Interferometer, Thruster electrodes, Rocket engines (JES)

19. ABSTRACT (Continue on reverse if necessary and identify by block number)

A new type of common path interferometer has been developed for use as a surface profilometer. The object beam and the reference beam remain coaxial (i.e., common path) all the way from the laser source up to the interference zone. This enables one to position surfaces to be profiled away from the optical head of the interferometer without having to compensate for any significant phase noise. A data acquisition/processing system capable of sampling at 30 kHz has also been developed to carry out the profilometry. Results of profilometry carried out using this system is reported. A new technique to heterodyne the coaxial beam interferometer is also proposed.

20. DISTRIBUTION/AVAILABILITY OF ABSTRACT	21. ABSTRACT SECURITY CLASSIFICATION
☒ UNCLASSIFIED/UNLIMITED ☒ SAME AS RPT. ☒ DTIC USERS	Unclassified
22a. NAME OF RESPONSIBLE INDIVIDUAL: Julian M Tishkoff	22b. TELEPHONE (Include Area Code): (202) 767-0465; 22c. OFFICE SYMBOL: AFOSR/NA

DD Form 1473, JUN 86 — Previous editions are obsolete. — SECURITY CLASSIFICATION OF THIS PAGE

Unclassified

NOMENCLATURE

E	=	amplitude of electric field
ϕ	=	phase of electric field
w	=	angular frequency
t	=	time
I	=	intensity of light
V	=	vivibility
S	=	signal at the detector
l	=	optical pathlength
λ	=	laser wavelength

Superscript

o	=	object beam
R	=	reference beam

Subscript

1 and 2	=	object and reference beam respectively
o	=	object beam
R	=	reference beam
A	=	detector A
B	=	detector B

TABLE OF CONTENTS

LIST OF FIGURES

1.0 WORK STATEMENT AND PROGRAM OBJECTIVES

1.1 Statement of the Problem

Material erosion at high temperatures occurs in various space and missile propulsion systems. For example, magneto-plasma-dynamic (MPD) thruster electrodes erode during operation in high-temperature plasma environments. Rocket engine nozzles also are subjected to erosive environments by particle laden combustion gases existing in the combustion chamber. Adequate methods for measuring erosion recession in hostile environments are not available to support development testing of propulsion systems. Some components of interest in space applications are required to have long life times (~ 10,000 hours or greater). Practical testing of such components require extremely sensitive methods to reduce test times to useful lengths. Present methods used to measure erosion recession include radioactive tracing and quartz crystal micro-balances. Both measurements are indirect insofar as they measure loss of mass rather than change in dimension and shape. They are also only used at specific points because they must be implanted into the surface of the material.

Thus, a direct measurement of the shape of the eroding material with sufficiently high resolution would present significant advantages, particularly if it could be used to measure a complete surface rather than a few specific points. The research that is being conducted under this program is anticipated to provide a fundamental understanding necessary for making such measurements with optical techniques.

1.2 Program Objective and Achievement

The aim of this research program is to investigate the possibilities of developing a noncontact optical technique by which surface erosion resulting from exposures to a high-temperature plasma environment can be monitored and measured. Three approaches; vis.,

a. Astigmatic Ranging Probe (ARP)
b. Holographic interferometry (HI)
c. Diffuse Point Interferometry (DPI)

were considered to have the potential to evolve into surface monitoring devices. However, early in the program it was realized that the ARP technique when applied to a rough surface was beset with serious signal-to-noise problems and, hence, was discarded.

As mentioned in the first annual report, a good part of the first year was spent developing the DPI technique and the preliminary results indicate that it can be a viable surface analysis tool provided it is ruggedized to be field worthy. In the second year of this program, we looked at the applicability of holographic interferometry to surface erosion study as well as ways to ruggedize the interferometer. Two types of HI, vis., real-time HI and sandwich HI were attempted. The former approach was besieged with problems such as rigid body motion, vibration and displacement gradients. Since we are attempting to measure small surface displacements (< .5 micron) out in the field, these problems would have confined this approach in the laboratory for a long time. The latter approach had to be given up because of inability to come up with a suitable reference surface (see Annual Report II for more details on this). Hence, once again our attention was turned to the interferometer.

The experimental setup of the Michelson interferometer during the first year of this study is shown in Figure 1. Since the object could not be brought any closer than 4", the reference beam and the object beam had to travel a minimum of 8" independently. In a field experiment this distance could be larger. Such an interferometer will respond to differential ambient perturbations seen by the two independent beam paths. This results in unwanted phase noise. Random phase excursions greater than 2π are possible for temperature differences of $\sim 1.44^{o}$ C between the two beam paths when they are separated by over 8 inches, (Figure 2). For an interferometer/optial profilometer, attempting to detect surface features of the order of λ, phase noise should be well under $\lambda/50$. Hence, we investigated ways to ruggedize the interferometer for use as a field-worthy surface profilometer. This search led us to the development of a simple common path interferometer. This interferometer has demonstrated its field-worthy capability, and has phase noise over two orders of magnitude smaller than that

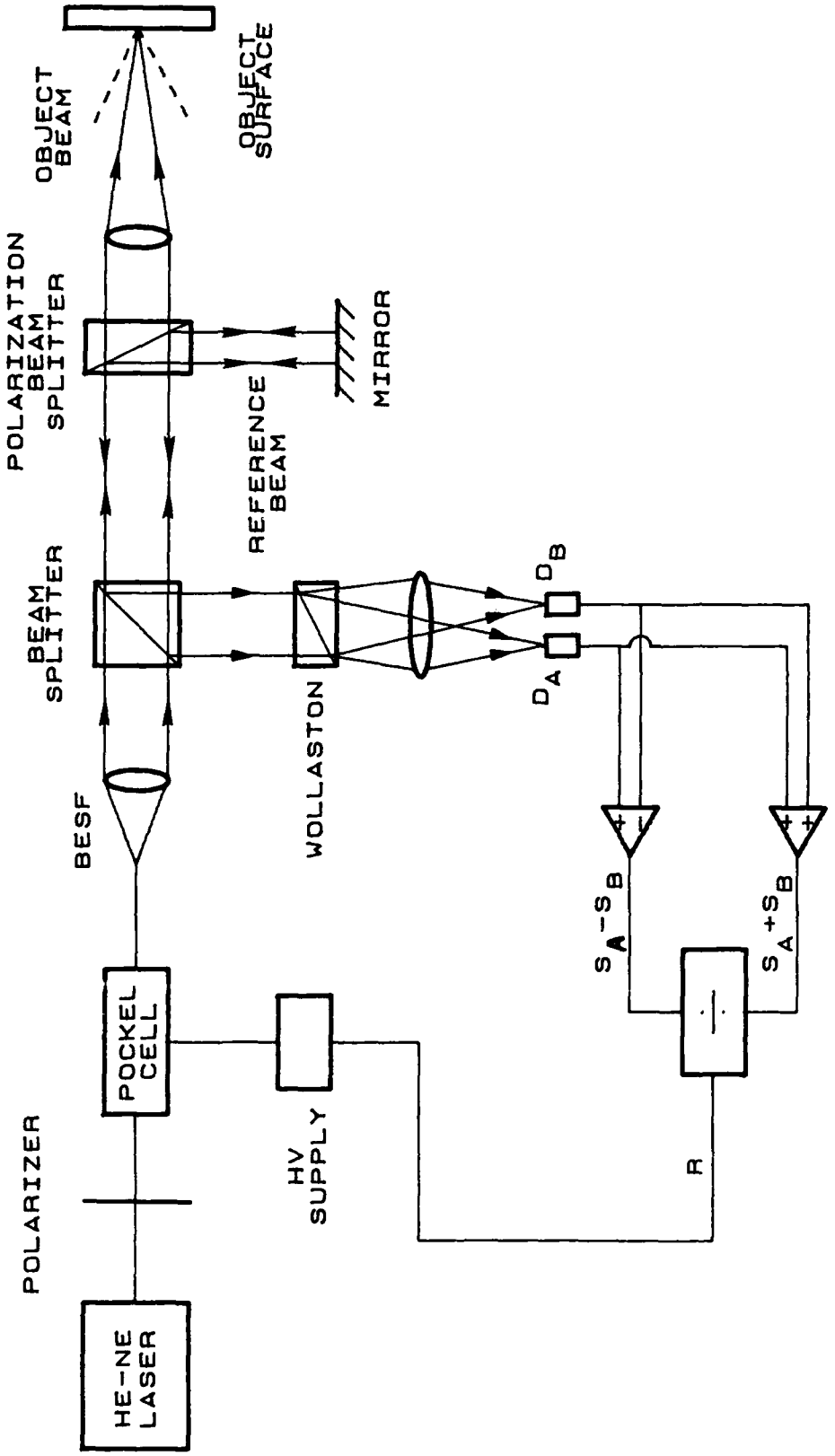

FIGURE 1. SCHEMATIC OF THE DIFFUSE POINT DIFFERENTIAL INTERFEROMETER

exhibited by the Michelson interferometer. In the next section we will describe this interferometer in detail.

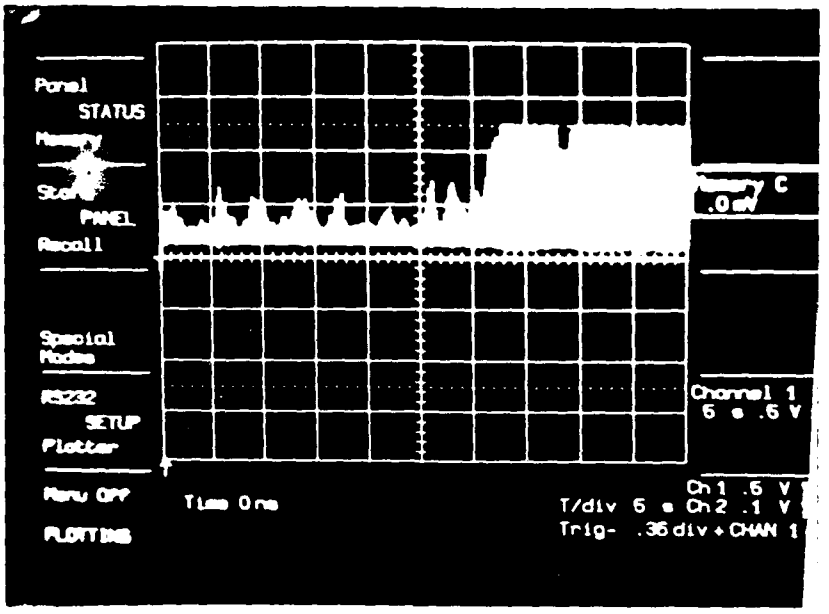

Figure 2. The CRT Display of Random Fluctuations in a Michelson's Interferometer Signal Resulting from Ambient Perturbation. Scales: 5 sec/div., 1 V/div.

2.0 COMMON PATH INTERFEROMETER FOR SURFACE PROFILOMETRY

A conventional interferometer of the Michelson or Mach-Zehnder type will be insensitive to external perturbations, (i.e., low-phase noise), if, and only if, both reference and object beams are subjected to identical perturbations or to no perturbations. However, in the real world, both situations are hard to realize, especially if the focusing optics in the object beam path have to be kept at a reasonable distance from the sample surface. (NOTE: Commercially available optical profilometers have the focusing lens within few millimeters of the sample.)

Minimizing the separation between the two beams will lead to a better signal-to-noise ratio. This separation is mainly determined by how close the interferometer can get to the surface and the need for path matching between the two beam paths. For the application that we are interested in, that is, profilometry of the inside surface of a magneto-plasma-dynamic thruster, the object beam, or probing beam, will be exposed to ambient environments, since a significant beam path length will be required to access the surface being profiled. Even in a laboratory environment, the Michelson signal showed considerable drift, (Figure 2). Since the signal will be much lower in strength compared to the drift, elimination of noise is absolutely essential for achieving subwavelength profiling capability. Suppression of noise through constant feedback, as is usually done in interferometry, is not possible in this situation, since the random noise (< 10 Hz) and the signal (pure dc) are in the same frequency regime. In situations where one cannot control the ambient perturbations and where feedback loops cannot be incorporated into the data acquisition system, the only way to significantly reduce the random phase noise, as mentioned above, is to subject both the reference and signal beams to identical perturbations. This can be achieved only when both arms travel the same path until the optical mixing occurs. A technique for achieving this is shown in Figure 3. After

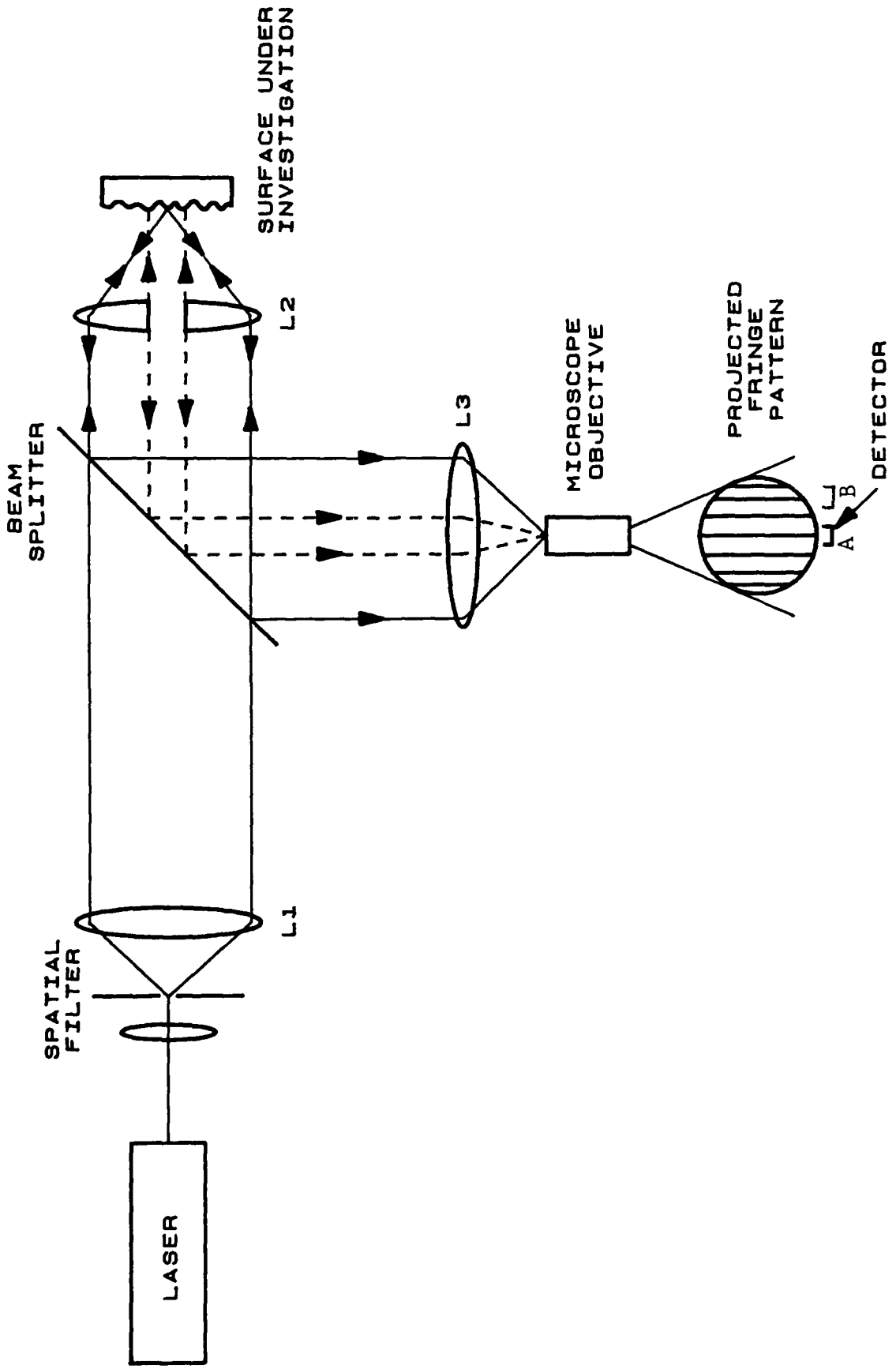

Figure 3. Schematic of the Single Beam Interferometer. In this Configuration, the Interferometer is Inert to Ambient Perturbations.

appropriate expansion and collimation the beam, it is split into an object beam and a reference beam at the lens. The part of the beam that gets through the hole in the lens acts as the reference beam, whereas the portion that gets focused by the lens is the object or probing beam. The object beam, because of its small dimension, carries local phase information upon return from the surface, whereas the reference beam wavefront returns with and average phase value which hardly undergoes any change as the beam is scanned across the surface (Figure 4).

The returning beams interfere at a small but finite angle and hence, closely spaced fringes are generated. For detection purposes, fringes will have to be projected, as shown in Figure 3. Signals obtained from this fringe system were found to be very stable compared to that from the Michelson interferometer as can be seen by comparing the signal in Figure 5 to that in Figure 2. The improvement in stability was found to be well over two orders of magnitude.

2.1 Analysis of Common Path Interferometry

At the interference zone, let $\overset{O}{E}_1$ and $\overset{R}{E}_2$ be the electric field strengths of the object and reference beams respectively. ϕ_O and ϕ_R are the phases associated with these two beams.

$$\overset{O}{E}_1 = \overset{O}{E}_{01}\, e^{i(wt + \phi_O)} \tag{1}$$

$$\overset{R}{E}_2 = \overset{R}{E}_{02}\, e^{i(wt + \phi_R)} \tag{2}$$

When the two beams interfere, the resultant intensity of the interference pattern is given by

$$I = \left(\overset{O}{E}_1 + \overset{R}{E}_2\right)\left(\overset{O}{E}_1 + \overset{R}{E}_2\right)^* \tag{3}$$

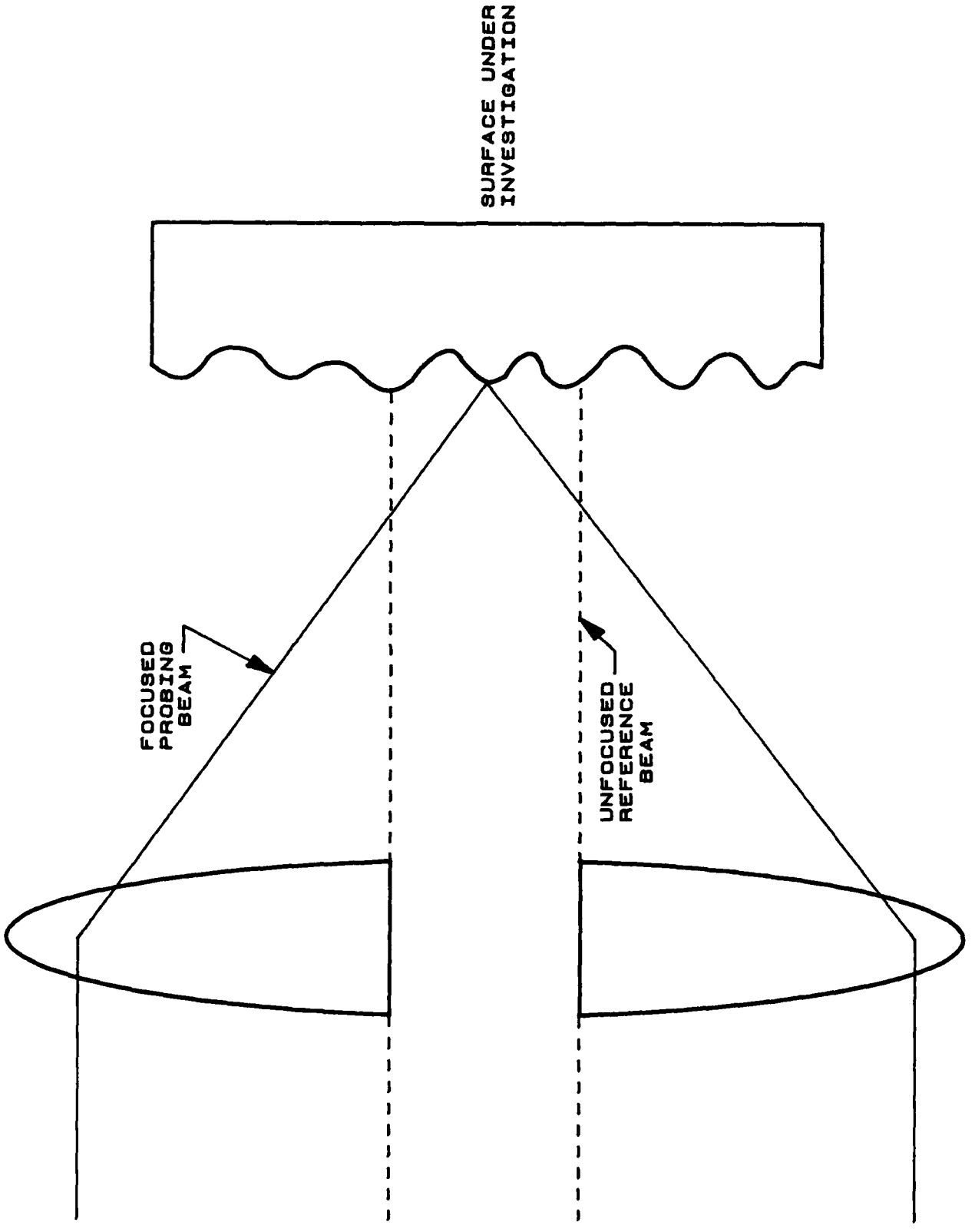

Figure 4. Geometry of the Reference Beam and Probing Beam on the Surface Under Test.

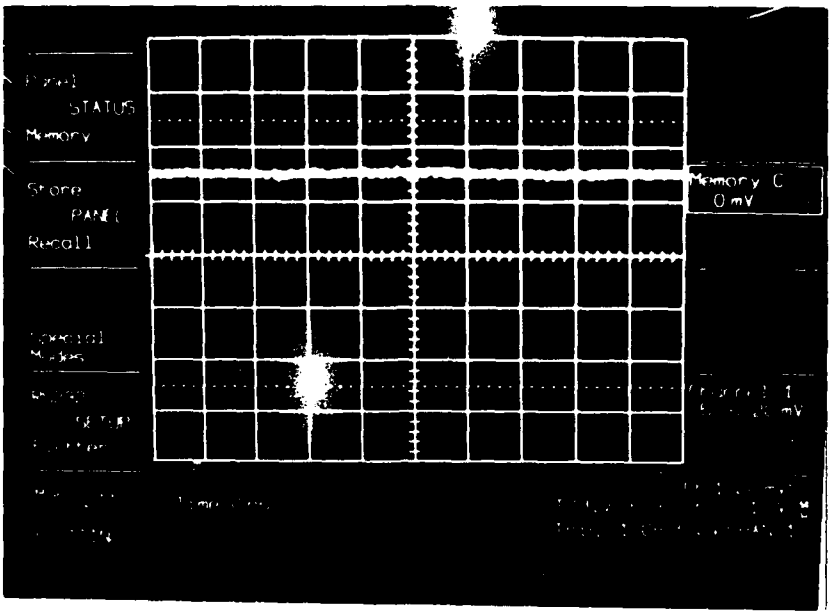

Figure 5. CRT Display of the Signal from the Common Path Interferometer. Scales: 0.5 sec/div., 20 mV/div.

Substituting (1) and (2) into (3), after appropriate manipulation, it can be shown that

$$I = \left(\overset{O}{E}_{01}\right)^2 + \left(\overset{R}{E}_{02}\right)^2 + 2\overset{O}{E}_{01}\,\overset{R}{E}_{0}\cos(\Delta\phi) \tag{4}$$

where $\Delta\phi = \phi_O - \phi_R$. Since intensity $I = E^2$, Equation (4) can be rewitten as

$$I = \overset{O}{I}_1 + \overset{R}{I}_2 + 2\left(\overset{O}{I}_1 \cdot \overset{R}{I}_2\right)^{1/2}\cos(\Delta\phi) \tag{5}$$

where $\overset{O}{I}_1$ and $\overset{R}{I}_2$ are the intensities of the object and reference beams.

Intensity of each fringe will be proportional to I. From (5), we get

$$I_{max} = \left[\overset{O}{I}_1 + \overset{R}{I}_2 - 2\left(\overset{O}{I}_1 \cdot \overset{R}{I}_2\right)^{1/2}\right] \tag{6}$$

and

$$I_{min} = \left[\overset{O}{I}_1 + \overset{R}{I}_2 - 2\left(\overset{O}{I}_1 \cdot \overset{R}{U}_2\right)^{1/2}\right] \tag{7}$$

and the visibility, V, is given by

$$V = \frac{I_{max} - I_{min}}{I_{max} + I_{min}} = \frac{2\left(\overset{O}{I}_1\,\overset{R}{I}_2\right)^{1/2}}{\overset{O}{I}_1 + \overset{R}{I}_2}$$

or

$$V \cdot \left(\overset{O}{I}_1 + \overset{O}{I}_2 \right) = 2\left(\overset{O}{I}_1 \overset{R}{I}_2 \right)^{1/2} \tag{8}$$

Using Equation (8), Equations (5), (6) and (7) can be rewritten as follows:

$$I = \overset{O}{I}_1 + \overset{R}{I}_2 + V \left(\overset{O}{I}_1 + \overset{R}{I}_2 \right) \cos\phi \tag{9}$$

$$I_{max} = \overset{O}{I}_1 + \overset{R}{I}_2 + V \left(\overset{O}{I}_1 + \overset{R}{I}_2 \right) \tag{10}$$

$$I_{min} = \overset{O}{I}_1 + \overset{R}{I}_2 - V \left(\overset{O}{I}_1 + \overset{R}{I}_2 \right) \tag{11}$$

For convenience sake $\Delta\phi$ is rewritten as ϕ, the value of which is needed for determining the profile of the surface under investigation.

The interference pattern is monitored using two detectors, A and B. The two are positioned such that their outputs are 180° out of phase. Hence, the signal generated by the two detectors can be expressed, based on Equation (9), as follows:

$$S_A = \overset{O}{S}_A \left[1 + V \cos \phi \right] \tag{12}$$

and

$$S_B = \overset{O}{S}_B \left[1 - V \cos \phi \right] \tag{13}$$

where $\overset{O}{S}_A \propto \overset{O}{I}_1 + \overset{R}{I}_2$ and $\overset{O}{S}_B \propto \overset{O}{I}_1 + \overset{R}{I}_2$.

If the two detectors have identical responses to the fringes, then

$$\overset{O}{S}_A = \overset{O}{S}_B = S_O \ .$$

Hence,

$$S_A = S_O \ [1 + V \cos \phi] \tag{14}$$

$$S_B = S_O \ [1 - V \cos \phi] \tag{15}$$

Therefore, from (14) and (15) the phase difference can be expressed as

$$\cos\phi = \frac{1}{V} \left[\frac{S_A - S_B}{S_A + S_B} \right] \ . \tag{16}$$

Since pathlength variation, $\Delta l = \frac{\lambda}{2\pi} \phi$, the dimension of a feature on the surface is

$$\Delta l = \frac{1}{2} \left[\frac{\lambda}{2\pi} \cos^{-1} \left\{ \frac{1}{V} \frac{S_A - S_B}{S_A + S_B} \right\} \right] \ . \tag{17}$$

The factor 1/2 appears because the beams travel twice the distance before interfering near the microscope objective.

The interferometer can be adjusted such that the phase difference, $\Delta\phi$, between the two beams at the start of the scan, is 90°, (called the quadrature point). This adjustment increases the sensitivity of detection. Features measured on the surface will be in relation to this starting point. For the above condition Equation (17) can be rewritten as:

$$\Delta l = \frac{1}{2}\left[\frac{\lambda}{2\pi}\sin^{-1}\left\{\frac{1}{V}\frac{S_A - S_B}{S_A + S_B}\right\}\right] . \tag{18}$$

For features with dimensions under $\lambda/50$,

$$\Delta l = \frac{1}{2}\ \frac{\lambda}{2\pi}\ \frac{1}{V}\left(\frac{S_A - S_B}{S_A + S_B}\right) . \tag{19}$$

From Equations (15) and (16), we have

$$S_A - S_B = 2\ V\cos\phi . \tag{20}$$

For measurements made about the quadrature point, (20) can be rewritten as

$$S_A - S_B = 2\ V\sin\left(\frac{2\pi}{\lambda}\ 2\Delta l\right) . \tag{21}$$

Where Δl is the path difference introduced by the features on the surface. For $\Delta l = l_O - l_R$, a positive value for (21) indicates a valley and a negative value means a peak. Thus, the sense of the features on the surface can also be determined with the

interferometer. However, it should be borne in mind that the dynamic range of the interferometer set at the quadrature point will be limited to $\lambda/2$.

Single Detector Approach

Surface profiling can also be achieved using just one detector, say A. The signal readout is

$$S_A = S_O \left[1 + V \cos \phi\right] .$$

The phase difference is

$$\Delta\phi = \cos^{-1} \left\{ \left(\frac{S_A}{S_O} - 1 \right) \frac{1}{V} \right\} , \tag{22}$$

Or, under quadrature conditions for small phase variations,

$$\Delta\phi = \frac{S_A - S_O}{S_O V} . \tag{23}$$

Where $(S_A - S_O)$ is the difference in signal between the starting point and the point under investigation in volts. Knowing the signal strengths corresponding to I_{max} and I_{min} and the visibility of the fringe system, S_O can be computed from Equation (10) or (11) in order to calculate $\Delta\phi$.

The two detector approach is preferable, since the ratio $(S_A - S_B)/(/S_A + S_B)$ is independent of any laser intensity fluctuations, and hence, it cannot influence the computed value of ϕ or Δl.

2.2 Signal Detection

The electronics circuit shown schematically in Figure 6, is designed to detect interference patterns with two detectors, A and B. The detectors are situated such that their output signals are 180 degrees apart in phase. The detected signals are then processed to provide phase information/path length variations resulting from the features on the surface of the test object.

The detectors that are used for this experiment are silicon detectors from United Detector Technologies. The active area of each detector is .020". This size was selected to match the fringe size and to avoid a possible dark current. Preliminary tests showed that the silicon detector performs better in a low frequency situation than a photomultiplier tube. The two signals, S_A and S_B, are fed into operation amplifiers, U1 and U3, respectively. Each amplifier, in conjunction with U2, provides a four-stage switchable amplifier. The different gain stages are 2x, 8x, 32x and 128x. These gain stages are matched on both four-stage amplifiers using precision resistors, within an error margin of 0.36%, (Table 1). The need for the switchable four-stage amplifiers is dictated by the expected range of signal strengths and the voltage ranges of the divider, U8.

Table 1

	Gain Stage	Gain	Input	Output	Error
Sig A				1746 mV	
	1	2x	895 mV		.3%
Sig B				1752 mV	
Sig A				1855 mV	
	2	8x	227 mV		.1%
Sig B				1853 mV	
Sig A				631 mV	
	3	32x	19.5 mV		.3%
Sig B				629 mV	
Sig A				1761 mV	
	4	128x	13.35 mV		.39%
Sig B				1754 mV	

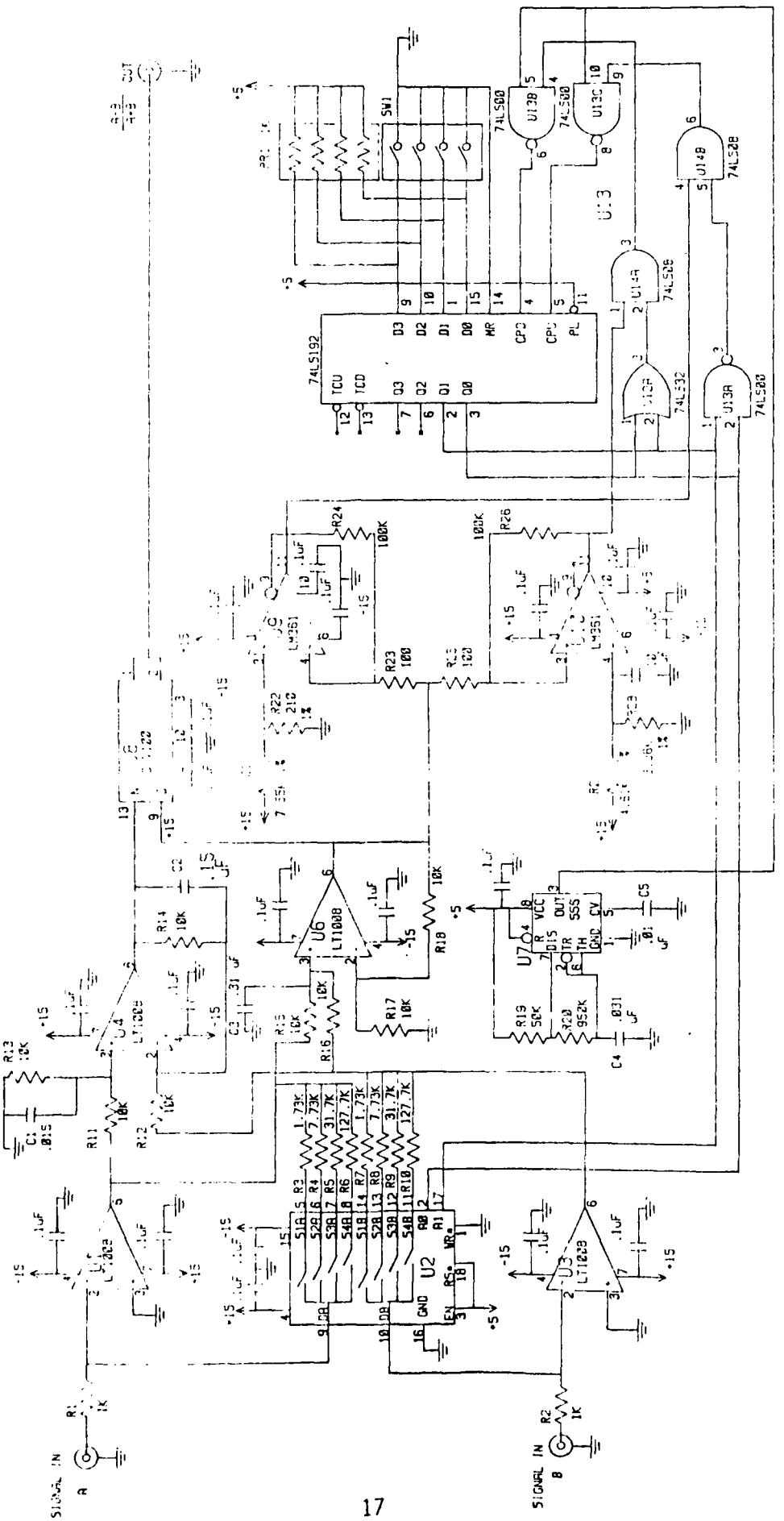

Figure 6. Schematic of the Detection Circuitry.

The outputs of amplifiers U1 and U3 are added in U6 to provide a signal, $S_A + S_B$, and subtracted in U4 to provide another signal, $S_A - S_B$. These two signals are then input to U8 to generate $(S_A - S_B)/(S_A + S_B)$. For the proper operation of the analog divider, the denominator $(S_A + S_B)$ should be greater than 250 mV or else a division by 0 occurs. To avoid this, the denominator is connected to a window comparator, U9, U10, so that it is kept between 395 mV and 6.32 V. The higher value is selected to stay within the output swing of the divider, which is maximum at 13V. An oscillator provides clock pulses every 1.59 ms to synchronize logic events. The window comparator controls the decision making logic which in turn signals U1 and U3 through the 'up-down' counter in U11, to change the gain stages up or down depending on the direction in which the denominator goes out of the window. An example of the performance of the comparators in conjunction with the logic circuit and the four-stage switchable amplifier is shown through the timing diagram in Figure 7.

The result $(S_A - S_B)/(S_A + S_B)$ obtained from the output of the divider is the signal that provides the phase change information. At the quadrature point, the output of U8 is zero. As the surface is scanned, the signal generated by U8 can be read using a CRT, as was done in generating the profile in Figure 8. This process is time consuming and the data recorded will be influenced by the slow drift in phase with time. The data can also be acquired using a PC, as described in the following section.

2.3 Data Acquisition System

To carry out profilometry, the surface under investigation will be moved across the beam. For this purpose, the surface was mounted on a translation stage that has a resolution of 1 μm. The object beam size on the surface is 20 μm. Hence, the surface was moved in steps of 20 μm. The interference pattern was monitored by two detectors, A and B. The signal from the detection system was fed to an A/D converter interfaced to a PC. Significant amounts of time had to be spent developing and debugging the interface software (see Appendix). Each

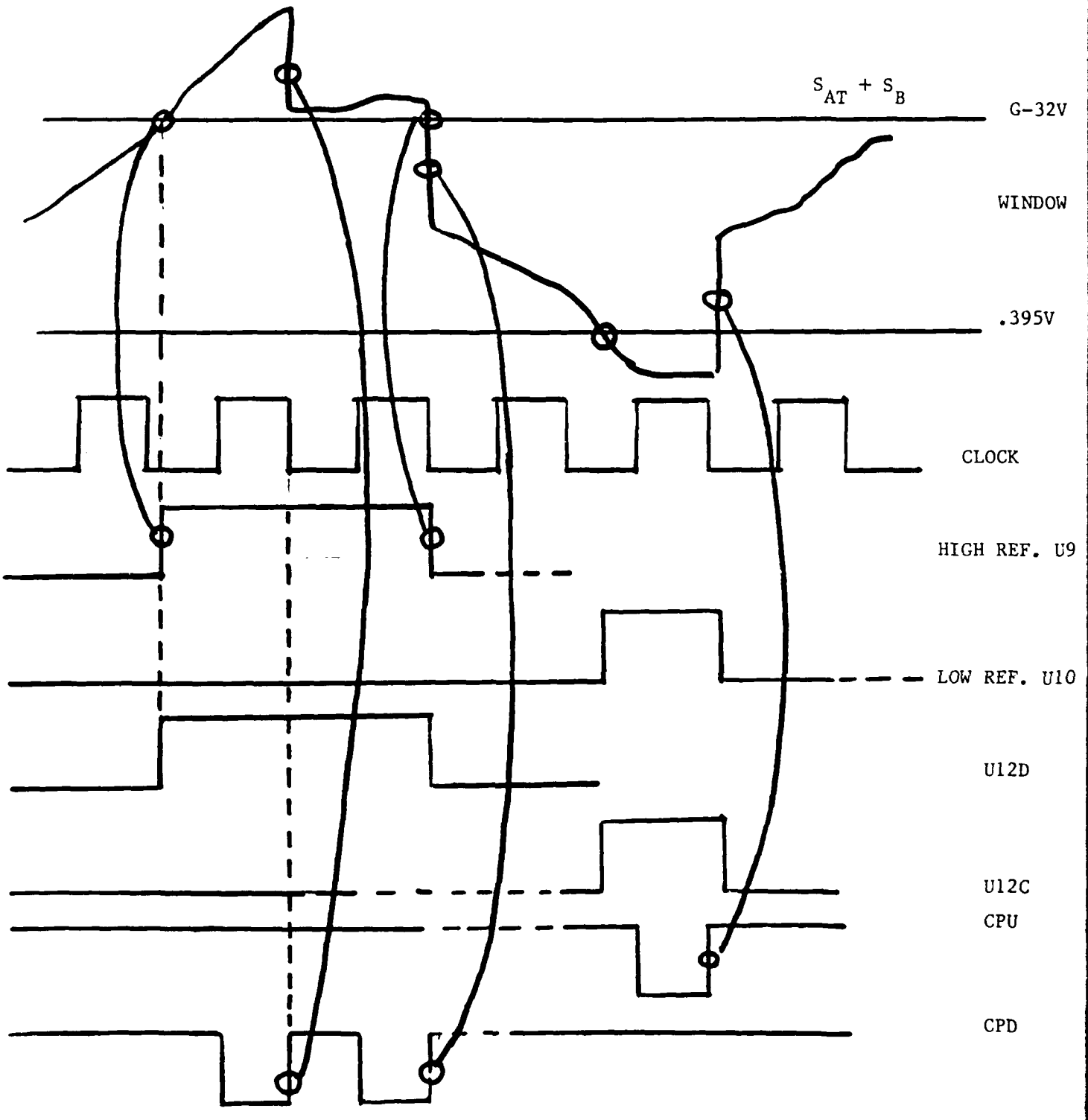

Figure 7. Timing Diagram

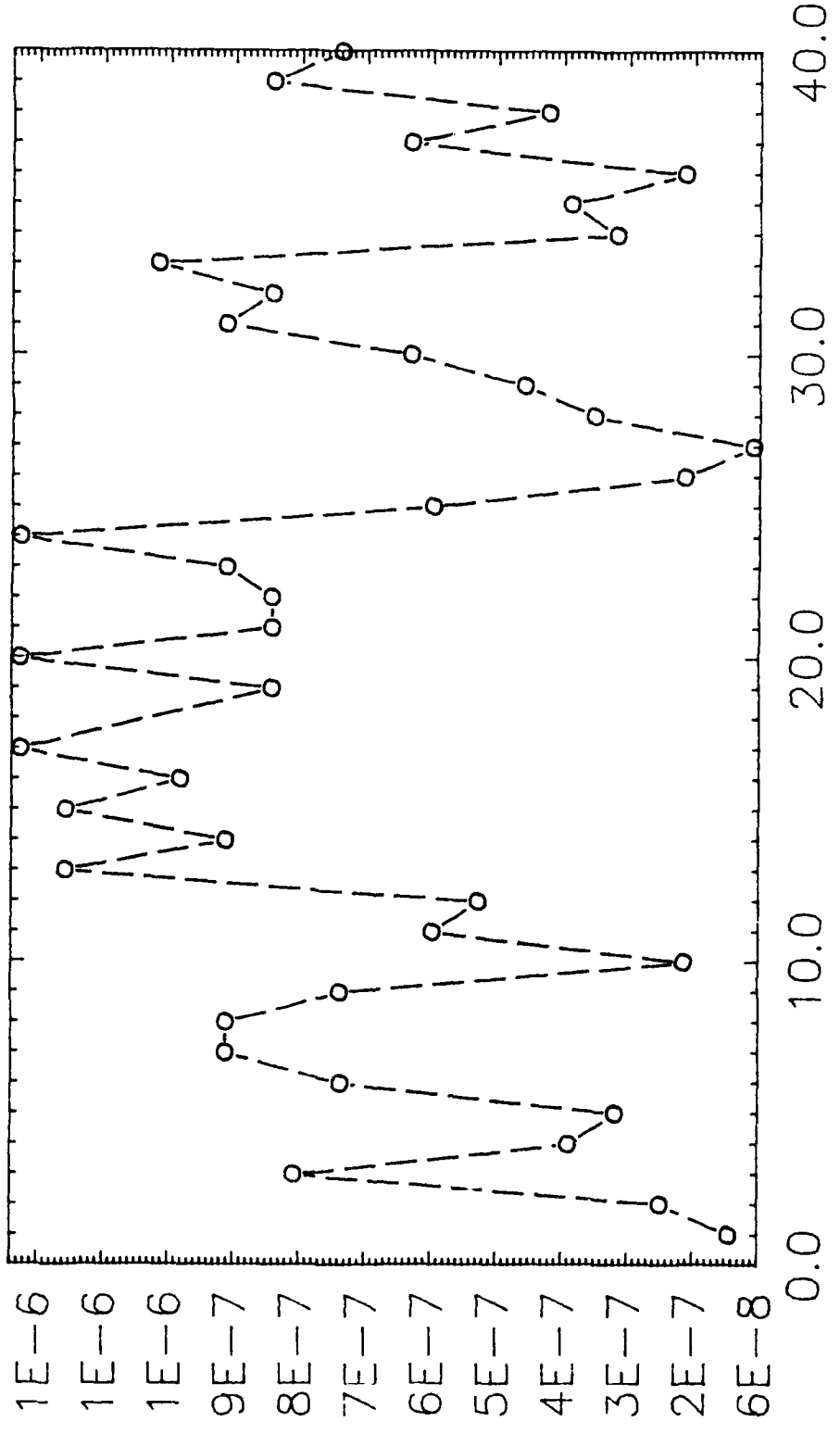

Figure 8. Plot of Surface Profile of a Standard Aluminum Mirror.

observation point was sampled 10,000 times. An average value of all the data along with the standard deviation value was calculated and stored in the memory. This process was continued as the surface being profiled was moved manually in steps of 20 microns. From the stored values of the ratio $(S_A - S_B)/(S_A + S_B)$, or from the ratio calculated using stored values of S_A and S_B, the dimension of the surface features Δl is calculated and then plotted.

Figure 9 gives a plot of the surface profile for a 1000 micron scan along a mirror surface for two data sets. The reproducibility of the data is quite good considering the fact that the interferometer was not shielded from air turbulence caused by the air conditioner in the laboratory. Figure 10 shows another profile taken at a different location on the mirror surface.

The upper limit of the interferometer was $\lambda/2$ and the detectability limit of the instrument was measured experimentally to the $\lambda/1000$ (Appendix B). A fringe counter is required to detect phase variations above $\lambda/2$. The information presented in Appendix B was obtained under another contract prior to our AFOSR contract.

After the initial testing of the interferometer, we attempted to profile the surface of a copper electrode. At this stage we ran into S/N problems due to poor reflectivity of Cu at the He-Ne wavelength. The laser we were using had an output power of 10 mW. A higher wattage laser could have alleviated the S/N problem somewhat. However, such a laser was not available to us and hence, we could not carry out any profilometry on a copper electrode surface. For future work with copper electrodes, we recommend using a diode laser at 0.83 μ. At this frequency, the reflectivity of copper is 25% more than that at the He-Ne wavelength. Moreover, the size of the diode laser can make the interferometer system compact, less bulky and easy to carry.

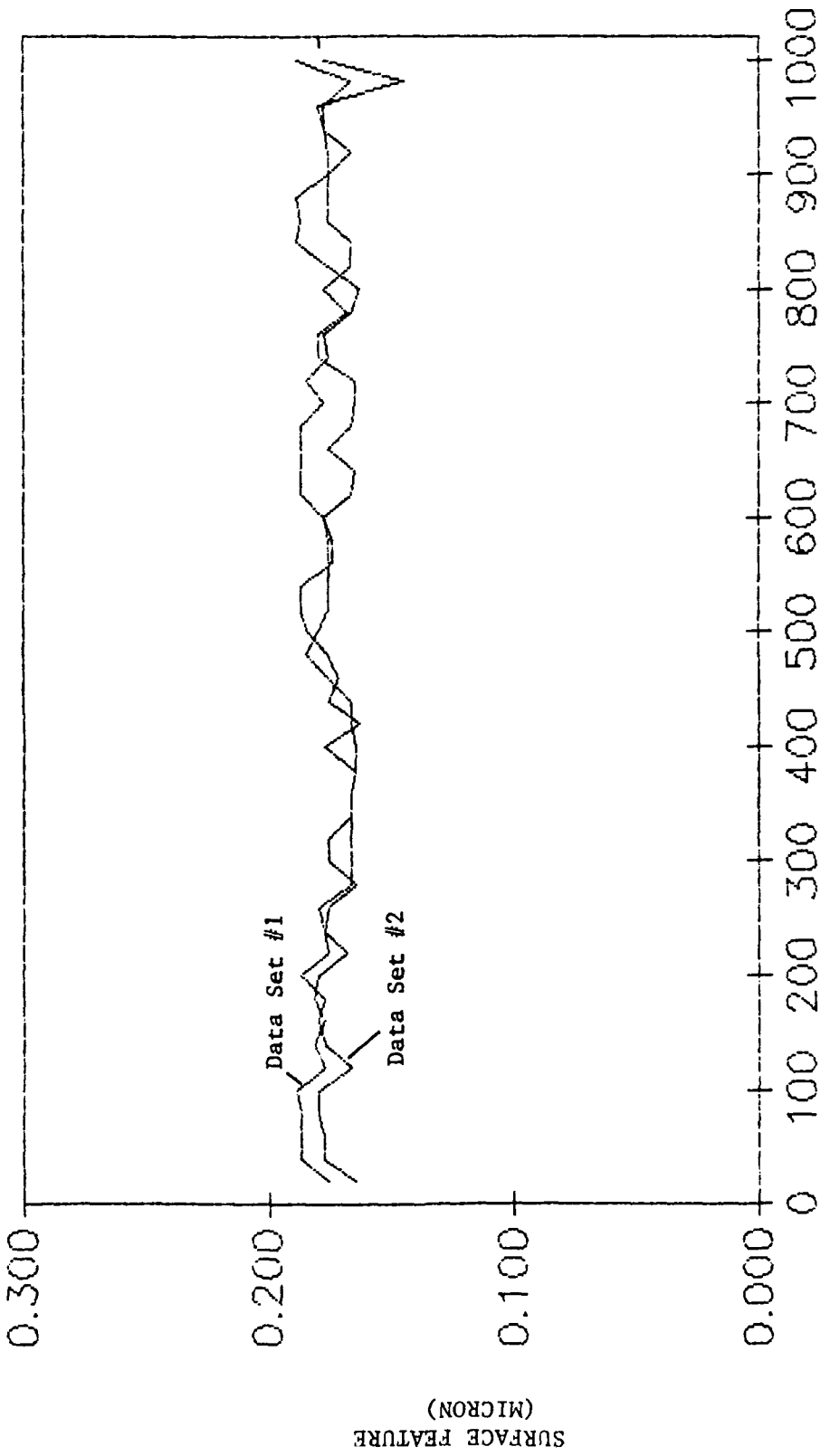

Figure 9. Surface Profile Carried Out with the Data Acquisition System

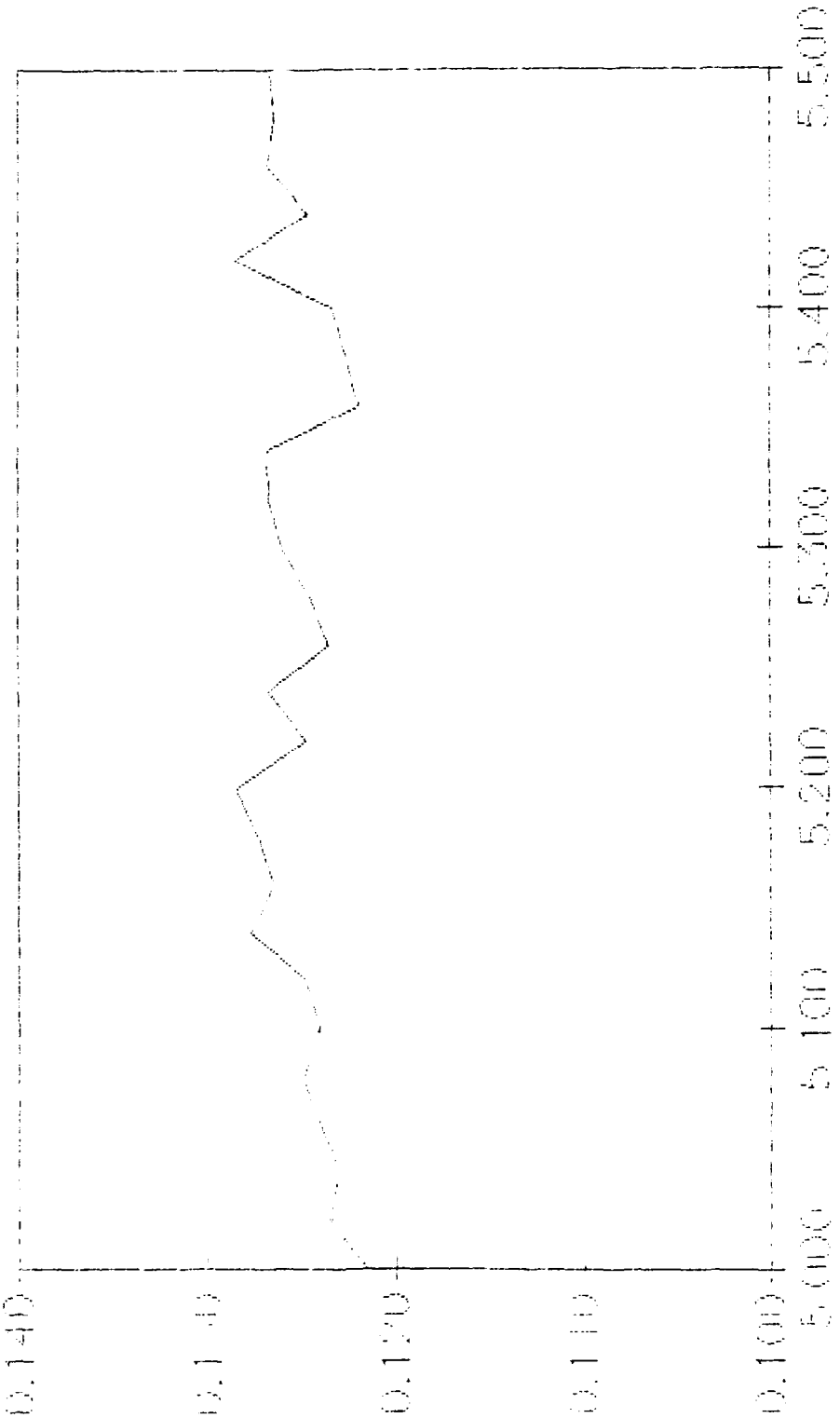

Figure 10. Surface Profile of Another Region of The Same Surface

3.0 PROPOSED HETERODYNE COMMON PATH INTERFEROMETER

Figure 11 represents the drift in the detector signal over a period of 1.67 hours. The drift frequency is typically ~ 500 μHz. This drift, though slow, can generate spurious signals during the measurement of small features. One way to get around this problem would be to speed up the data acquisition process and also implement a heterodyne detection technique. In order to achieve heterodyning, either the object beam or the reference beam must be frequency shifted by an amount, $\Delta\upsilon$. When the two beams are recombined, the resulting interference pattern sweeps across the field of view of the detector face at a frequency equal to $\Delta\upsilon$. The sinusoidal signal thus generated can be filtered from any random noise that may be present. The filtered signal can thus be used in conjunction with a phase meter to detect phase difference between the two beams.

In a classical Michelson or Mach-Zehnder interferometer, heterodyning is easily achieved since the object and reference beams travel independent paths. However, in the commonpath interferometer which we have developed, the reference and object beams are coaxial and, hence, standard techniques employed to shift the frequency of one with respect to the other cannot be applied and a new technique will have to be developed to achieve the necessary heterodyning. We intend to frequency shift the central 2 mm diameter portion of a 12 mm diameter beam using a series of wave plates. The approach to achieve this unique form of heterodyning is shown schematically in Figure 12. A combination of two quarter-wave plates will be positioned such that the inner 2 mm diameter of the output beam will be circularly polarized, whereas the outer tubular part of the beam will have its e-vector perpendicular to the plane of the paper. This beam then passes through a spinning two $\lambda/2$ plate combination (Figure 12) such that the circularly polarized part of the beam experiences a phase retardation of $\pi/2$. This changes the sense of rotation of the e-vector of the circularly polarized part of the beam. In addition, this part of the beam also suffers a frequency shift

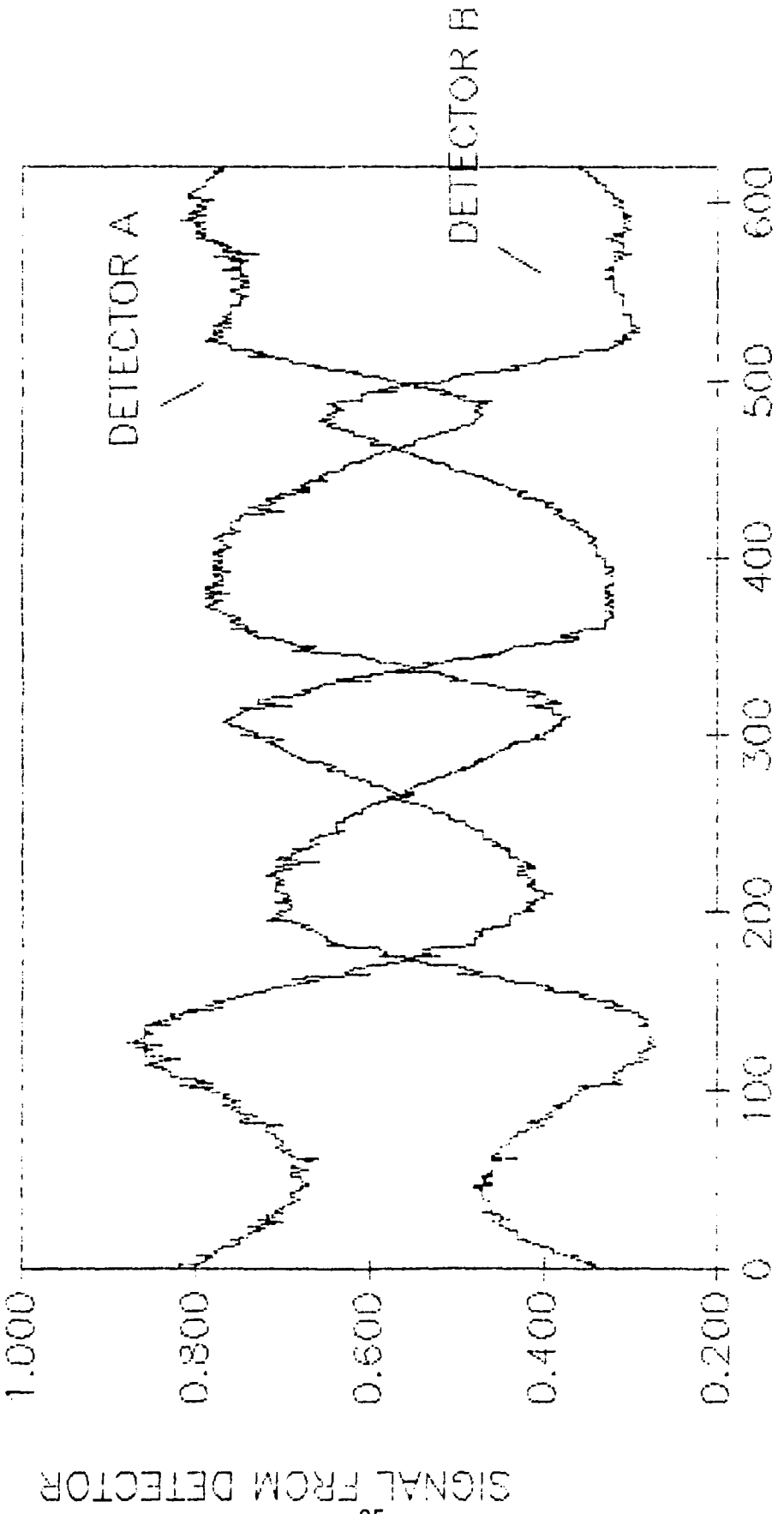

Figure 11. Plot of the Signal Drift In The Common Path Interferometer.
Drift Frequency 500 Hz.

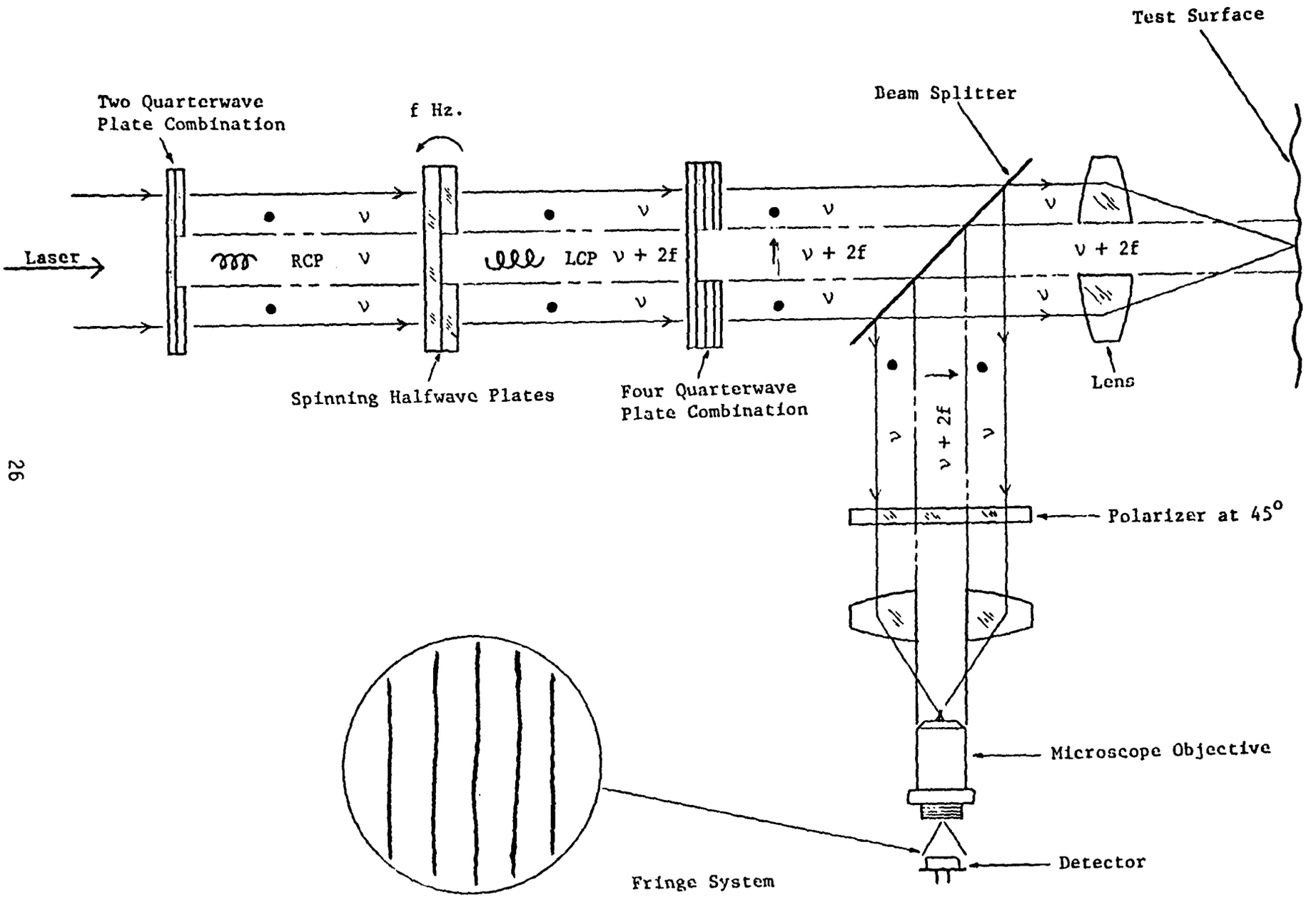

87-1161pp

Figure 12. Proposed Heterodyne Commonpath Interferometer.

equal to twice the spin frequency since half-wave plates, by nature, introduce a 2θ rotation of the eigenvector, θ being the angle between the optical axis and the electric field vector.

Next, the beam goes through a combination of four $\pi/4$ plates such that the center portion of the beam undergoes a $\pi/2$ phase change while the outer part of the beam suffers no net phase retardation. The resulting light is a coaxially birefringent ray (COBRA) with its central part frequency shifted with respect to the rest of the beam.

After passing through a beam splitter, the COBRA passes through a lens that has a hole through the center. The frequency shifted part of the beam goes through the hole while the unshifted part is focused by the lens. For interferometric purposes, the unfocused beam will act as the reference beam and the focused beam will be the probing or profiling object beam. Since the object and reference beams have orthogonal polarization, no interference effect will occur on the test surface. The returning beams are then passed through a polarizer of appropriate orientation to generate uniform polarization across the beam diameter. Using the proper optics, an interference pattern that responds to the features on the test surface can be generated.

Since the object and reference beams are separated in frequency, the detector signal will exhibit sinusoidal behavior at 2f Hz, which can be filtered from the random noise due to environmental perturbations. This signal will then be sent through a phase meter, where the path length difference between the two beams will be detected. We expect that through this approach, one should be able to profile a surface down to few angstroms, even in a hostile environment.

4.0 CONCLUSIONS

The conclusions based on the results of the work done during the course of this program are as follows:

1. Serious signal-to-noise ratio problem limits the applicability of an astigmatic probe to the study of surface erosion.
2. Because of its sensitivity to the environmental perturbations, it was determined that holographic interferometry was not a viable technique for monitoring erosion in electrical propulsion under real test conditions.
3. A new type of common path interferometer was developed to carry out surface profilometry.
4. The common path interferometer has demonstrated its field-worthy capability.
5. Profilometry of copper electrodes could not be achieved due to poor return signal. It is expected that this problem can be overcome by using 0.83 μm radiation from a diode laser, instead of the 0.63 μm from a He-Ne laser.
6. A technique to heterodyne the common path interferometer has been proposed. This approach is expected to increase detection sensitivity.

5.0 TECHNICAL ARTICLE IN PREPARATION

"A Novel Approach to Common Path Interferometry," to be submitted to Applied Optics.

6.0 LIST OF PERSONNEL ASSOCIATED WITH THE PROGRAM

The scientists involved in this program are:

K. A. Arunkumar	Senior Scientist
M. Azzazy	Senior Scientist
C. Fitzpatrick	Senior Scientist
L. E. Hurtado	Electronics Engineer
D. Y. Lee	Scientist
M. Petros	Technician
J. D. Trolinger	Chief Scientist

7.0 PAPER PRESENTED AT MEETINGS, CONFERENCES, SEMINARS, ETC.

The results of our work was presented at the Fifth Annual Meeting of SEM in Costa Mesa, CA on March 22, 1988.

8.0 NEW DISCOVERIES, INVENTIONS OR PATENT DISCLOSURES AT SPECIFIC APPLICATIONS STEMMING FROM THE RESEARCH EFFORT

The newly developed DIP interferometer can be applied to surface measurements where high accuracy is needed. We are looking at the possibility of patenting this interferometer.

8.1 Highlights of the Common Path Interferometer

The interferometer, without heterodyning, and without any isolation from ambient perturbations, is found to be capable of detecting submicron surface features. With the introduction of heterodyning and improved detection electronics, we feel its sensitivity can be pushed to the angstrom level.

The common beam path provides remarkable fringe stability and makes the interferometer ideally suited for field and production line measurements. Hence, we anticipate potential applications for this interferometry in many scientific and industrial realms.

APPENDIX A

Listing of file: b:start.c
1/01/80 0:06 AM

```
/*
*  This program is a system's check program to determine the proper
*  functioning of the 30 kHz A/D converter board from Metra byte.
*  It will be used on the surface roughness interferometer which has
*  a 100 Hz bandwidth and maximun voltage swing of +/- 5.0 v.
*  We are going to collect data coming from to channels at the maximun
*  digitization rate possible.
*  The program will initialize the board and then proceed to collect
*  10 000 samples, storing them in a memory array, and performing a
*  arithmetic average when the acquisition is over. The result will
*  be stored on disk for archival purposes.
*/


        #include        <conio.h>
        #include        <math.h>
        #include        <stdio.h>
        #include        <stdlib.h>

                /*  adc board port addresses */
        #define             AD_8    0x300           /*  do a 8 bit conversion */
        #define             AD_12   0x301           /*  do a 12 bit conversion */
        #define             COMD    0x302           /*  adc command register */
        #define             DATM    0x300           /*  adc data register */
        #define             STAT    0x302           /*  adc status register */
        #define             CKCMD   0x307           /*  timer's control register
*/
        #define             CKFRQ   0x306           /*  timer 2 data register */
        #define             OC_CLK  0x304           /*  timer 0 data register */

                /*  adc status test flags */
        #define             RD_WT   0x80            /*  end of conversion flag */
        #define             IRQ     0x08            /*  interrupt flag */
        #define             DUMMY   0               /*  irrelevant data */

                /*  other constants */
        #define             VmaX    10              /* peak input voltage */
        #define             StrCH   1               /* mux starting channel */
        #define             EndCH   2               /* mux final channel */
        #define             CHNL    2               /* number of channels */
        #define             SAMPLE  500             /* total number of samples */
        #define             GEN     0xb6            /* rate gen load lo/hi byte *
/
        #define             RATE    2000            /* 2 kHz sampling rate */
        #define             FACTOR  0.0024414               /* adc lsb resolution
  */
        #define             SizE    8000            /* number of points *
        #define             TRUE    1
        #define             FALSE   0
        #define             MAx     0xfff           /* allowed limit range */
        #define             MIN     0
```

```
    int buffer [ CHNL] [ SIZE];

    main()
  {
   FILE *fg;
   char line[40];
   int channel, clock, delay, eoc, sample;
   int byt_rd, maxval= MIN, minval= MAX;
   unsigned int i, j;
   unsigned long int total;

   float average, plainx, std_dev, valx;
   double sigma, squarex;

   union adc {
         unsigned int c;
         unsigned char ch[2];
         };
   union adc dat, freq;


/*       input filename    */
/*    printf( "give filename < [dev:][path]name.ext > = ");
*    scanf("%s",line);
*    printf("\n");*/

/*       initialize the clock rate */
    outp( CKCMD, GEN );           /* set counter2 to generate pulses */
    freq.c = RATE;                /* with a 2 MHz rate and do loading */
    outp( CKFRQ, freq.ch[0] );    /* in a double byte transfer mode*/
    outp( CKFRQ, freq.ch[1] );

/*       access file for data manipulation        */
    if (( fg = fopen( "data" , "a+")) == NULL)
         perror( "couldn't open data file");


     for ( sample=0; sample<SAMPLE; sample++ ) {
         channel = StrCH;                  /* select starting channel */

/*  poll clock for positive edge occurrence */
/*       while ( ( clock = inp ( STAT ) & IRQ) != TRUE)   * wait for sampling c
lock edge */
         do {
                   outp( COMD, channel );           /* pick the channel number */
                   delay = 0x0003;                  /* let the multiplexer settle
 */
                   while (delay != 0)               /* for 2 us */
                   {       delay--;
                           }
```

```
                outp( AD_12, DUMMY );              /* perform 12 bit digitizatio
n */
                while ( ( eoc = inp( STAT ) & RD_WT) != FALSE)  /* wait for e
nd of conversion */
                dat.ch[0] = inp( DATM);            /* get the lower bits */
                dat.ch[1] = inp( DATM+1 );         /* now comes the upper bits *
/
                dat.c >>= 4;                       /* shift right 4 bits */

                buffer[ channel-1][ sample] = dat.c;     /* store value in arr
ay */
                channel++;                         /* update channel number */
        } while ( channel != EndCH+1 );
    }

/*      perform calculations on array    */
        for( j=StrCH-1; j<EndCH; j++) {

        plainx = 0.0;
        squarex = 0.0;
        total = 0;

           for( i=0; i<SAMPLE; i++) {
                if ( buffer[j][i] > maxval) maxval = buffer[j][i];
                if ( buffer[j][i] < minval) minval = buffer[j][i];

/*      make converted number into signed number */
                valx = (float)buffer[j][i] * FACTOR - ( (float) VmaX/ 2);
                plainx = plainx + valx;
                squarex = squarex + ( valx*valx);
                total++;
           }

        average = plainx / total;
        sigma = ( squarex - (plainx*plainx/total)) / (total-1);
        std_dev = sqrt( sigma);
        printf( " average value= %-13.2g     std deviation= %-13.3g \n",
                                average, std_dev);
        fprintf( fg, "%-13.2g%-13.3g\n", average, std_dev);
        }

    fclose(fg);
    printf( " that's all folks! \n");
 }
```

SBE PROJECT PLAN AND REVIEW

Project No./Title: 2439-High Temp. Material Erosion
P.I.: KAA
Contract Amount: $295711
Target Cost: $278224
Target MOC:
Target Labor:
Start Date:
End Date: 8/31/88

Projected: ● or ____
Actual: ▲ or ____

% Completion - Indicate by shading in blocks.

PROJECT ELEMENTS
Common Path Interferometer Setup
Develop Data Acquisition Hardware/Software
Carry Out Experiments

0 10 20 30 40 50 60 70 80 90 100

MONTHS

Oct Nov Dec Jan Feb Mar Apr May Jun Jul Aug Sep

DELIVERABLES	Dates Planned/Actual
Final Report	5/1/88 | 8/31/88

278
270
262
254
246
238
230
Cost ($K)

SDL PROJECT PLAN AND REVIEW

Project No./Title: 2439 AFOSR-High Temp. Material Erosion.
P.I.: KAA
Contract Amount: $295,711.00
Target Cost: 272,795.00
Target MOC:
Target Labor:
Start Date: 01 March 1985
End Date: 31 March 1988

Projected: ● or - - - - -
Actual: ▲ or ——

% Completion - Indicate by shading in blocks.

PROJECT ELEMENTS
Holography Set-up
Real Time HI on Electrode
Data Analysis
Sandwich Holography on Electrode
Data Analysis
Semi-Annual Report
Diffuse Point Interferometer Set-up
Ruggedization - Initial Results
Second Annual Report

DELIVERABLES	Dates Planned/Actual	
Second Annual Report	4/1/87	4/17/87

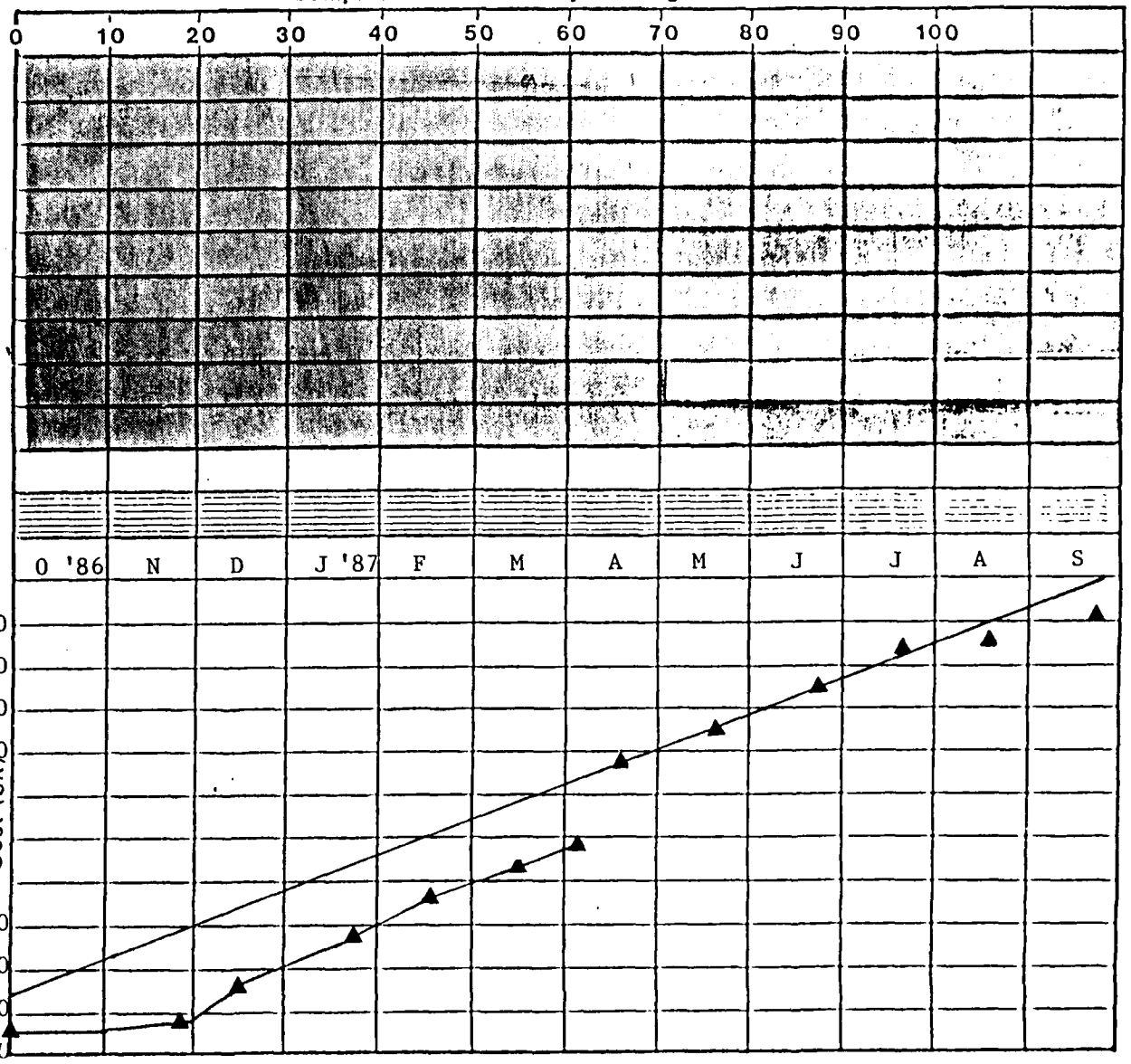

APPENDIX B

Optics and Lasers in Engineering **10** (1989) 000–000

Surface Topography Using Diffuse Point Differential Interferometry

M. Azzazy

Spectron Development Laboratories Inc., 3535 Hyland Avenue, Suite 102, Costa Mesa, California 92626, USA

(Received 22 September 1987; revised version received and accepted 25 January 1988)

Optics and Lasers 35818(OLE 0042)

ABSTRACT

A high sensitivity non-contact optical profilometer based on diffuse point differential interferometry has been developed and used to measure the surface profile of camshafts. The high sensitivity of the system is achieved through differential detection of the interference patterns of the scattered light. An electronic phase-lock feedback loop is used to control the quadrature condition and determine the surface height. Preliminary measurements show that the interferometer system is sensitive to surface height variations in the order of 0·002 μm. The influence of the surface speckles on the interference pattern is analyzed, and the performance of the diffuse point differential interferometer is evaluated. The system has the advantage of not having any moving mechanical parts which leads to fast and more accurate measurements of the surface contours.

1 INTRODUCTION

Measuring the surface profile of diffuse objects is imperative to many engineering fields. Today, the common practice in industry is to contour the surface using mechanical profilometers,[1,2] which often utilize diamond styluses that contact the surface. Although diamond styluses have the potential of contouring the surface of diffuse objects with high sensitivity and good spatial resolution, they suffer the drawback of causing damage to the surface being inspected as well as wear to the probe tip. Furthermore, any misalignment in positioning

the probe tip may result in serious damage to both the probe and the inspected surface.

To overcome this problem several non-contact optical techniques have been developed. These techniques may vary from the point of view of simplicity, accuracy and applications. Techniques based on Mirau heterodyne interferometry[3] have a height sensitivity of about 1 Å rms. However, those techniques require comparing the test surface to a reference surface which limits their applications. Nomarski differential interference contrast (DIC)[4] has a height sensitivity of about 10 Å. The technique measures the slope of surface heights which can then be converted into the surface profile. Although electron micrograph techniques[5] are used to measure the 2-dimensional surface profile with a sensitivity of about 10 Å, data reduction is very complicated and requires calibration with a well-known surface profile. Optical heterodyne interferometry techniques[6] yield high sensitivity (1 Å) but are limited to targets with simple geometry and highly specular surface characteristics. Stereo photography, moiré, and point triangulation techniques[7–9] suffer from lack of accuracy and require complex image processing to reduce raw data. Astigmatic probes,[10] while simple and accurate at normal incidence, exhibit reduced accuracy when the probe beam strikes the target surface at oblique incidence angles. Speckle interferometry[11] techniques are capable of measuring rms surface roughness in the order of 10 Å.

In the present work we describe a non-contact method which is capable of measuring diffuse surface profiles without mechanically moving any optical components. The method utilizes two beams of orthogonal polarization. The object beam, which is scattered by the diffuse surface, and the reference beam, are made to interfere at the plane of a detector via a Wollaston prism whose optical axis bisects the angle between the two planes of polarization. The phase-lock loop which comprises a Pockels cell, a differential amplifier, and a high voltage power supply, is then used to compensate the phase difference due to surface roughness. The technique does not require any surface preparation and is capable of measuring diffuse surface profiles with a sensitivity as high as 0·002 μm. Since the surface profile is measured directly, the autocovariance function, spectral density function, and statistical properties of the surface can be determined analytically.[12]

2 PRINCIPLE OF OPERATION

The interferometer system, in principle, is a variation of Smeets and George interferometer.[13,14] The instrument optical system is illustrated

in Fig. 1. A Wollaston prism, Wollaston (1), is used to split a linearly polarized laser beam into two plane polarized beams (S and P polarizations). The polarization direction and orientation of the optical axis of the components in the system are crucial to the performance of the interferometer. In the present configuration, the original polarization direction of the laser beam was at 45° with respect to the scattering plane, which is defined as the plane that contains the direction of laser beam propagation and the detector. The optical axis of Wollaston (1) and the Pockels cell were perpendicular to the scattering plane. One beam is then focused onto the diffuse surface while the other is focused onto a mirror. The scattered and reflected light is then collected and recombined by Wollaston (1). No interference is possible at this stage since the two beams are of opposite polarization. The remainder of the detection system involves another Wollaston prism, Wollaston (2), whose optical axis is oriented at 45° with respect to Wollaston (1). This orientation results in interference of the two beams at the detector plane.

The interference patterns of the two beams emanating from Wollaston (2) are detected by a quadrant detector. The two signals A and B are 180° out of phase, that is

$$I_A = I_0 + I_1 \cos(\phi + \gamma)$$
$$I_B = I_0 - I_1 \cos(\phi + \gamma) \tag{1}$$

where ϕ is the optical phase difference of the two beams and γ the phase introduced by the Pockels cell. The amplitudes I_0 and I_1 are proportional to the laser power and visibility. The signals I_A and I_B are combined in a differential amplifier to produce a signal proportional to the cosine of the phase difference, that is

$$I_c = 2I_1 \cos(\phi + \gamma) \tag{2}$$

The quadrature condition is achieved when $\phi + \gamma = \pi/2 + 2m\pi$. The feedback loop used in this study is phase tracking homodyne detection system (PTMDS). The output signal I_c is normalized by the sum signal, $I_A + I_B$, to reduce the effect of laser power drift. The normalized signal is then used as an error signal to drive the Pockels cell. The quadrature condition is realized when the difference signal is null. Under this condition, the phase introduced by the Pockels cell is equal in magnitude to the phase introduced by the surface roughness. Therefore, surface contours can be determined by measuring the optical path retardation in the Pockels cell.

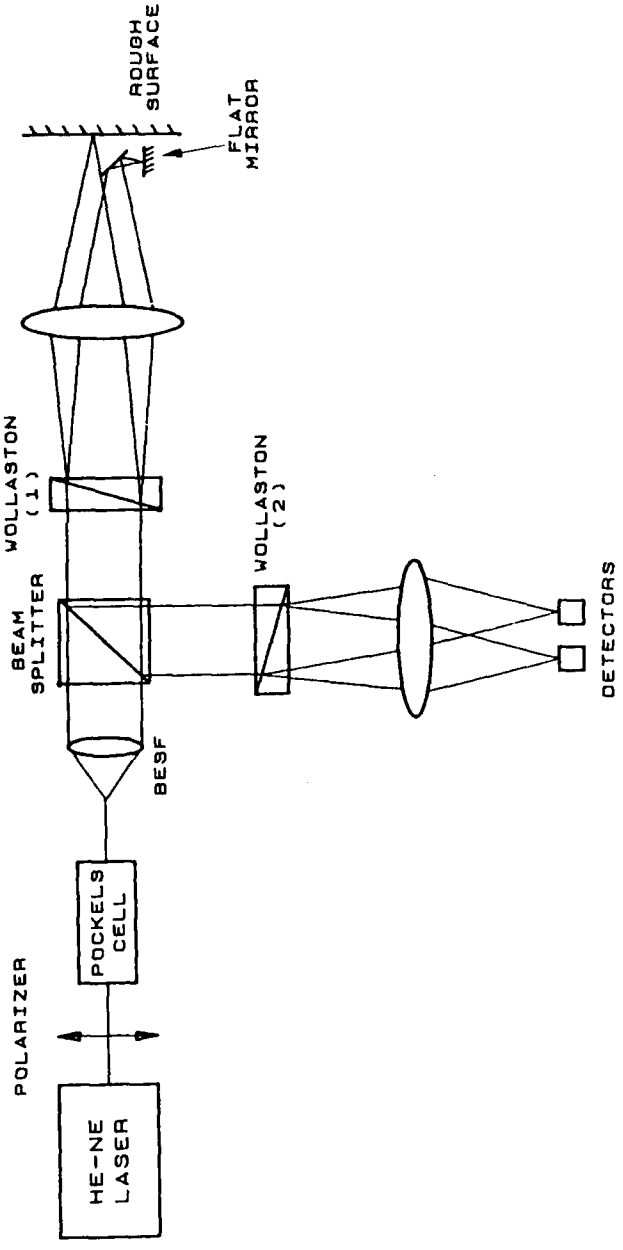

Fig. 1. Schematic diagram of the optical system.

3 EXPERIMENTAL APPARATUS AND RESULTS

The performance of the interferometer system was characterized by its ability to follow surface profiles sensitivity, and accuracy.

The ability of the system to follow surface profiles of diffuse objects was established in 2 steps. In both steps the reference beam was reflected from a polarization sensitive mirror. A differential micrometer with a sensitivity of 0·25 μm was utilized to mount the surface used to reflect/scatter the object beam. The first step involved using a mirror to reflect the object beam while in the second step a polished piece of aluminum was used. The supply voltages to the Pockels cell are plotted against the micrometer reading in Fig. 2. This linear behavior allows the measurement of surface contours.

Figure 2 also shows that interference can be made between scattered light from a diffuse surface and reflected light from a mirror. Moreover, the interferometer system followed the linear displacement of the diffuse surface in a manner similar to the specular mirror. The mathematical verification of these conclusions will be given in section 4.

The sensitivity and accuracy of the system were characterized by artifically introducing a pathlength disturbance to one of the arms of the interferometer and measuring the resulting signal. In order to introduce pathlength variations of the order of $\lambda/500$ that can be independently measured with high accuracy, a temperature-controlled shear layer was designed. Fluid temperature fluctuations of 1 °C over a distance of 1·0 cm were introduced over one of the arms of the interferometer. This disturbance is equivalent to pathlength variations of the order of 0·002 μm. Figure 3 is a schematic of the apparatus. The temperature fluctuations were measured using a cold wire anemometer and the interferometer simultaneously. A complete description of the shear layer and the optical system is given elsewhere.[15] Figure 4 shows the relationship between the interferometer signal strength and the path-length difference. The sensitivity of the differential interferometer system was found to be of the order of 0·002 μm.

Figure 5a is a sample of the surface contour of an injector lobe after the process of grinding. Cam scans were made every 1·6 mm. Figure 5b shows the same surface profile measured by the 'Universal Machine', a mechanical profilometer. No direct comparison between the two figures was attempted at this stage; however, the rms roughness obtained from the interferometer was 0·645 μm, and the mechanical profilometer was 0·652 μm.

Figures 6 and 7 show the surface profile of a cam lobe after the process of polishing and etching, respectively. The rms roughness

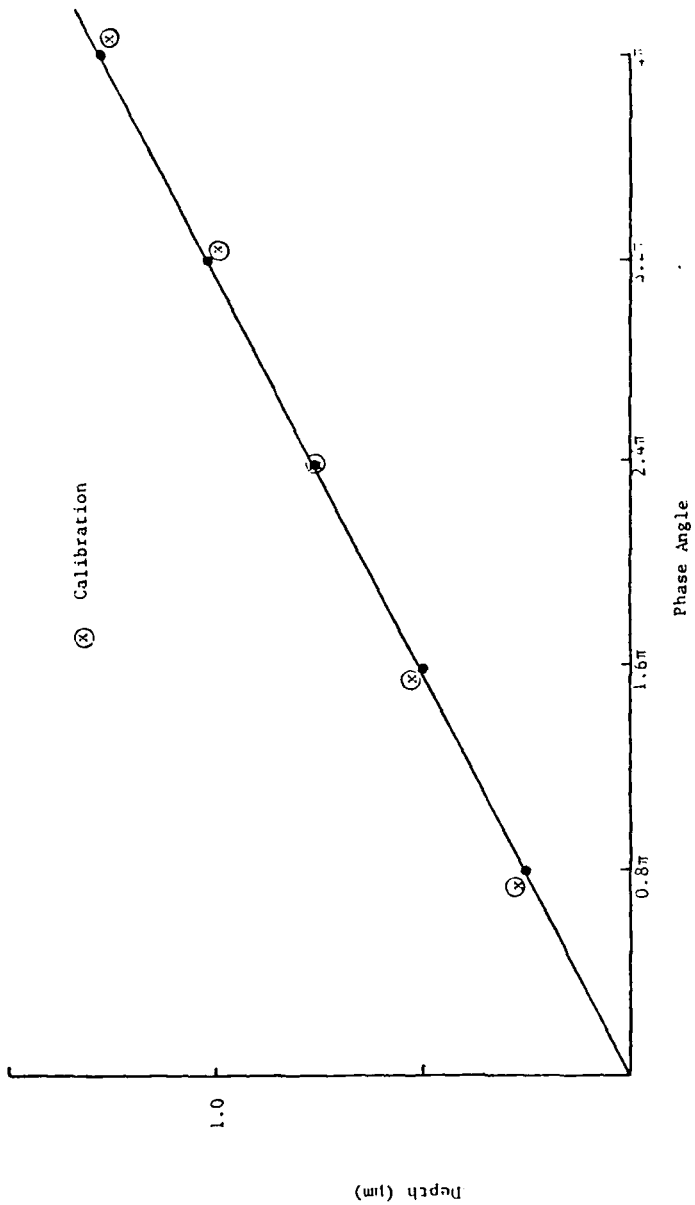

Fig. 2. Calibration of the diffuse point differential interferometer.

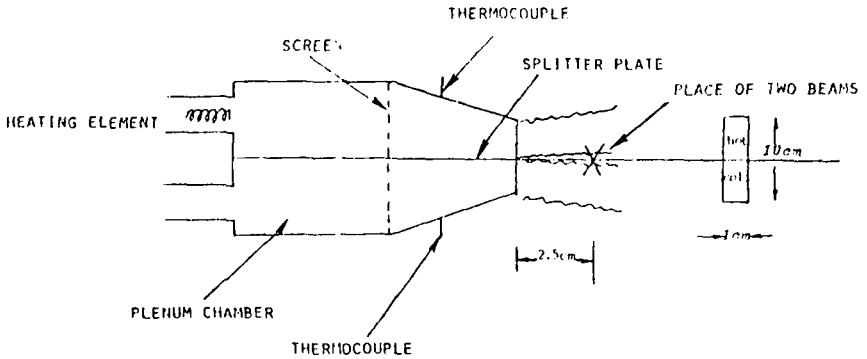

Fig. 3. Schematic of the shear layer assembly.

obtained from the interferometer and the mechanical profilometer were 0·262 μm and 0·259 μm, respectively for Figs 6a, and 6b and 0·290 μm and 0·293 μm, respectively for Figs 7a and 7b.

4 MATHEMATICAL ANALYSIS

4.1. Specular surface

Using Jones's calculus,[16] the electric field entering through Wollaston (1) can be presented as

$$E_m = e^{i(\omega t + kz)}\begin{bmatrix} a_s e^{ik\gamma} \\ 0 \end{bmatrix} + \begin{bmatrix} 0 \\ a_p \end{bmatrix} \tag{3}$$

where ω is the laser frequency, k the wave number, γ the phase introduced by the Pockels cell, and a_s and a_p the amplitude of the electric field in the S and P polarization directions, respectively. After passing through Wollaston (1) the electric field amplitude, E_m, remains the same provided that the optical axis of Wollaston (1) and the Pockels cell are parallel. The scattered light, E_{sc}, from the surface can be represented by a deterministic complex function ρ, describing the reflectance of the surface (amplitude) and profile (phase) such that

$$E_{sc} = \rho E_m \tag{4}$$

where the complex function ρ is defined as

$$\rho = \begin{bmatrix} e^{ik\delta_s} & 0 \\ 0 & e^{ik\delta_p} \end{bmatrix} \tag{5}$$

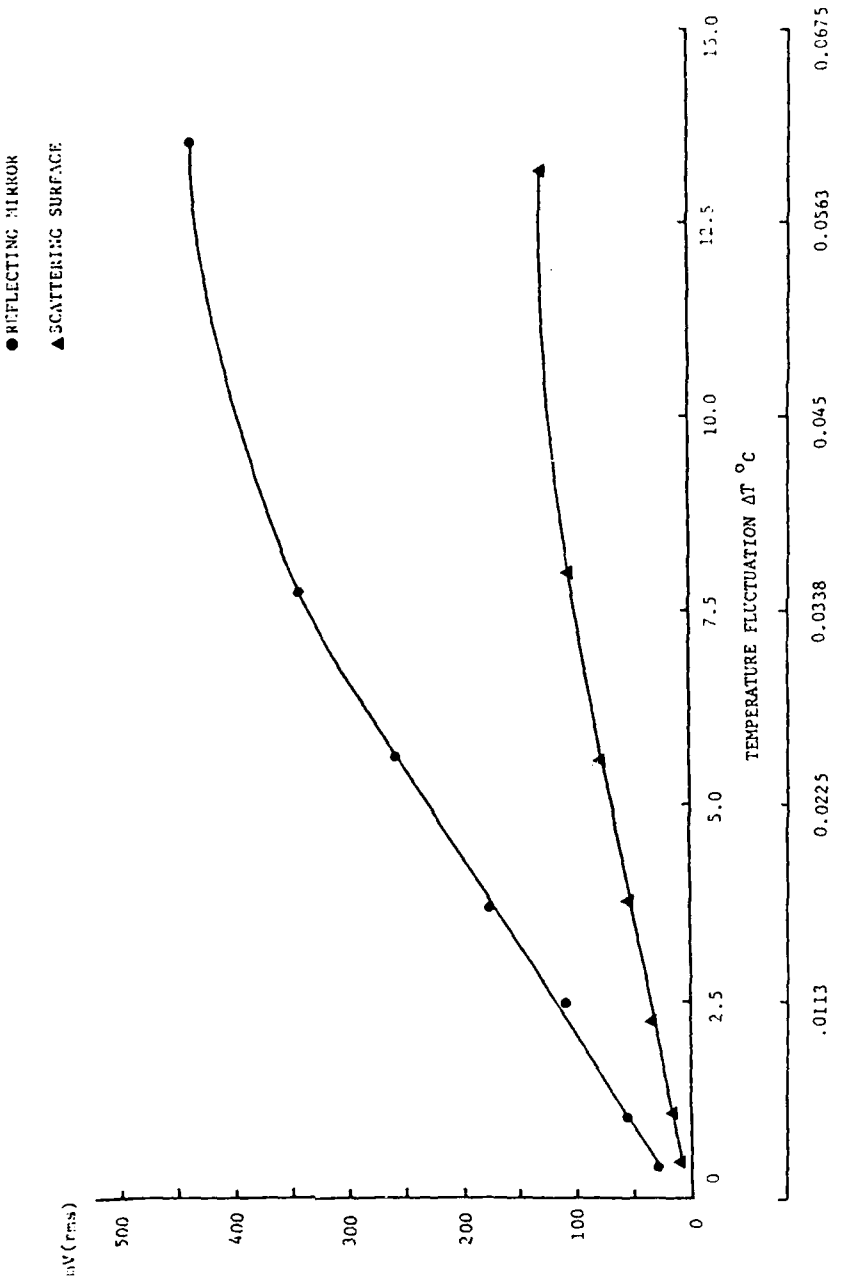

Fig. 4. Laser interferometer signal rms as a function of temperature fluctuation for both the reflecting mirror and the scattering surface.

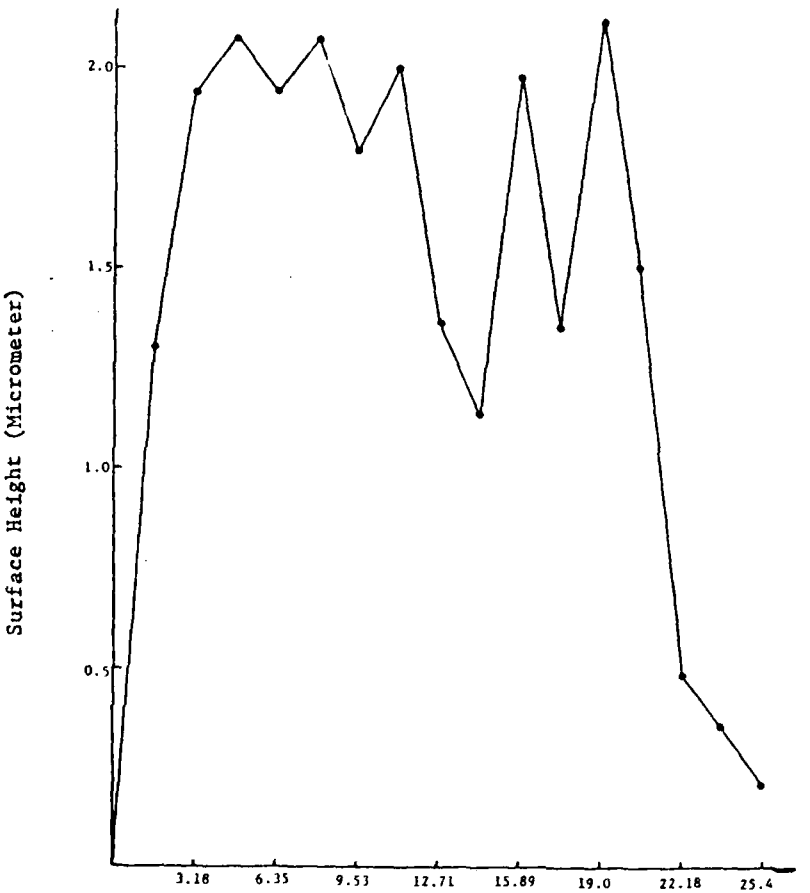

Fig. 5a. Injector lobe surface profile after grinding process using diffuse point differential interferometry.

where δ_y and δ_x are the disturbances in the optical pathlength of the inspected surface and reference beam, respectively. In this case, the phase difference $\delta = \delta_x - \delta_y$ represents twice the change in optical pathlength due to surface height.

Since Wollaston (2) is oriented at 45° to Wollaston (1) an interference pattern will occur in the plane of the photodetectors. Using the coordinate system illustrated in Fig. 2, the electric field amplitude at the detector plane, E_{sig}, will be

$$E_{sig} = \frac{1}{\sqrt{2}} \begin{bmatrix} 1 & 1 \\ 1 & -1 \end{bmatrix} \begin{bmatrix} E_{sc1} \\ E_{sc2} \end{bmatrix} \tag{6}$$

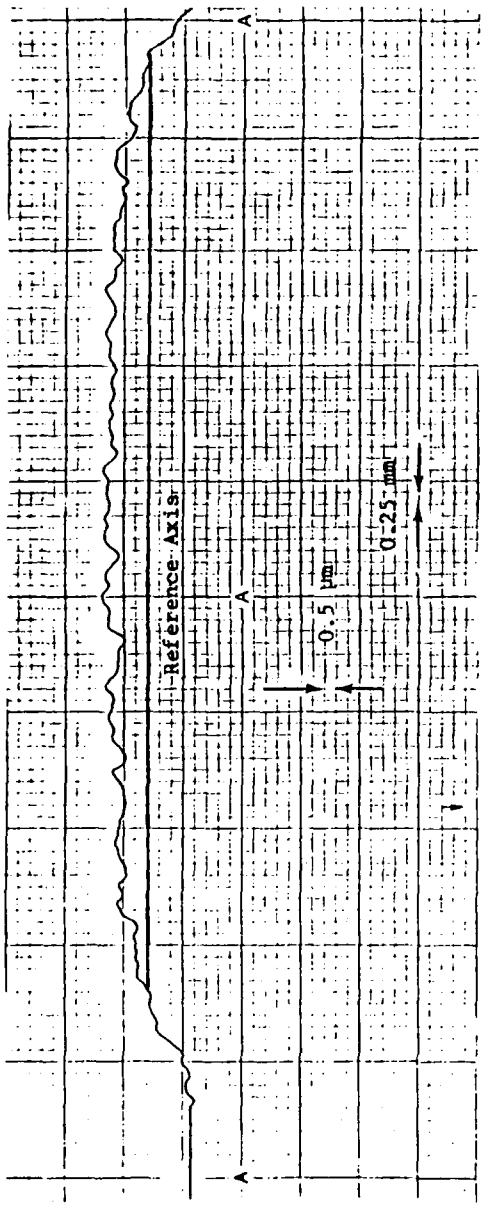

Fig. 5b. Injector lobe surface profile after grinding process using a mechanical stylus.

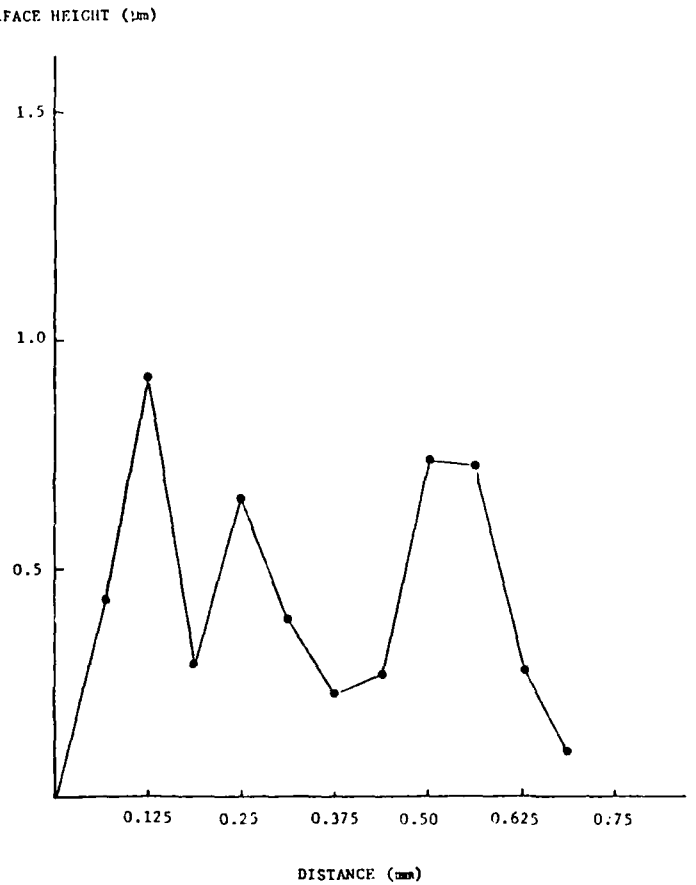

Fig. 6a. Cam surface profile after polishing process using diffuse point differential interferometry. Surface height rms value = 0·262 μm.

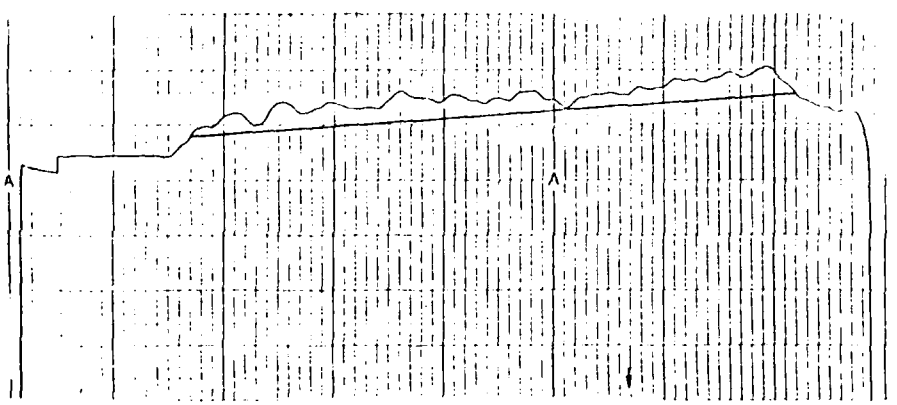

Fig. 6b. Cam surface profile after polishing process using a mechanical stylus. Surface height rms value = 0·259 μm.

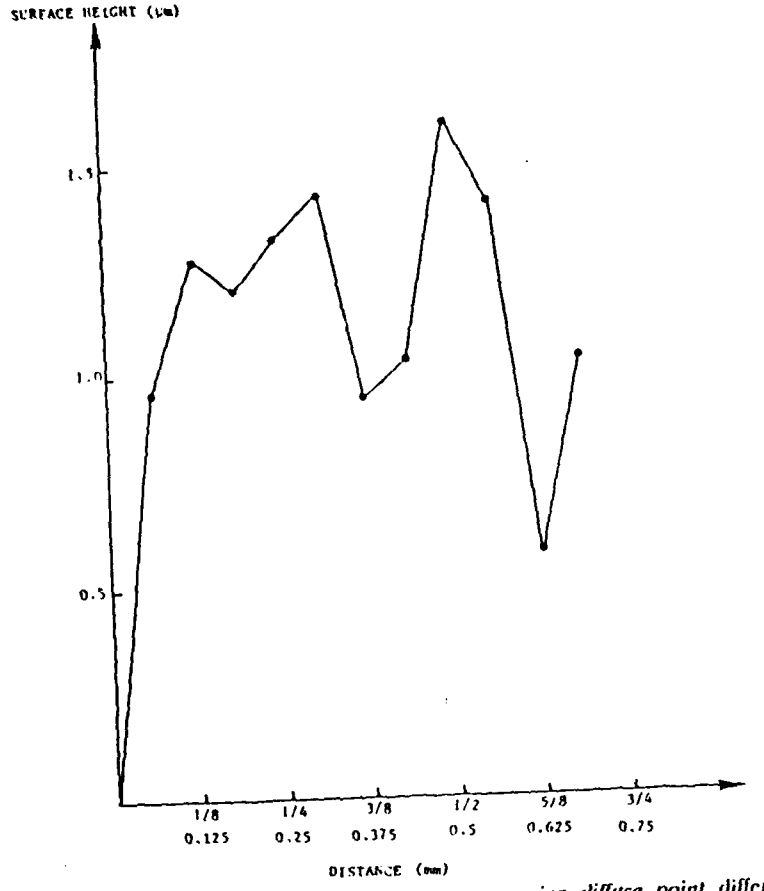

Fig. 7a. Cam surface profile after etching process using *diffuse point differential* interferometry. Surface height rms value = 0·290 μm.

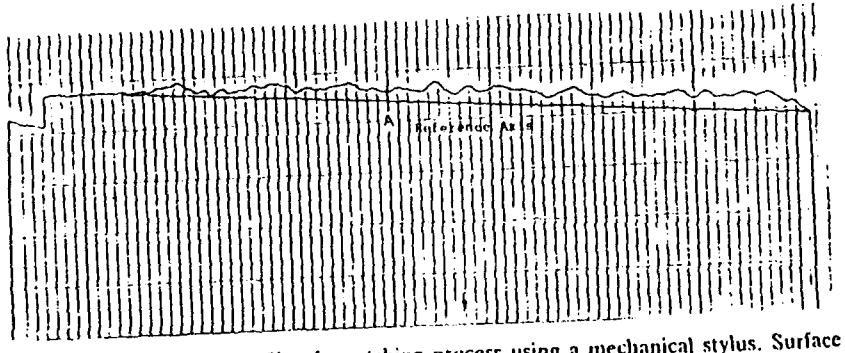

Fig. 7b. Cam surface profile after etching process using a mechanical stylus. Surface height rms value = 0·293 μm.

After algebraic manipulation the detector signals become

$$S = S_0\begin{bmatrix}1\\1\end{bmatrix} + S_0 V\cos[k(\delta+\gamma)]\begin{bmatrix}1\\-1\end{bmatrix} \tag{7}$$

where $S_0 = a_s^2 + a_p^2$ is the laser power, and $V = 2a_s a_p/S_0$ is the fringe visibility.

The familiar quadrature condition is achieved when the phase is odd multiples of $\pi/2$, i.e.

$$k(\delta+\gamma) = (2n+1)\frac{\pi}{2} \qquad n = 0, 1, 2, \ldots \tag{8}$$

An error signal, $S_- = S_1 - S_2$, where S_1 and S_2 are the detector signals expressed by eqn. (7), is used to control the phase difference, γ, introduced by the Pockels cell to ensure that the quadrature condition, eqn (8), is realized. Thus, the phase difference will be

$$\delta = \frac{\lambda}{4} - \gamma \tag{9}$$

where λ is the laser wavelength. Since the phase, γ, is linearly proportional to the supply voltage to the Pockels cell, the surface heights, $\delta/2$, can be obtained by measuring the supply voltage to the Pockels cell.

4.2 Diffuse surface

Diffuse objects acquire a peculiar granular appearance, known as speckle, when viewed with highly coherent light.[17] The nature of the speckle pattern (i.e. the size and shape of each speckle), can be described by the intensity correlation function.[18] Since the minimum deconvolution area of a given surface is of the order of λ, the maximum number of individual scatterers in the illuminated area is of the order of $(d_0/\lambda)^2$ where d_0 is the minimum beam diameter at the surface. In our case the maximum number of scatterers was 900. In order to study the influence of speckles on the interference pattern, assume that the incident laser beam can be divided into a number of coherent wavelets. Each wavelet is equal in size to the minimum deconvolution area. The surface profile within that area is assumed to be constant.

Therefore, the scattered light from the surface will be the sum over all the scatterers.

$$E_{sc} = \rho' E_m \tag{10}$$

where the complex function ρ' is defined as

$$\rho' = \begin{bmatrix} e^{ik\delta_1} & 0 \\ 0 & e^{ik\delta_n} \end{bmatrix} \tag{11}$$

where δ_n is the disturbance in the optical path length due to wavelet n. Following the same analysis as in the previous section the detector signals after dropping the time dependance will be:

x'-direction

$$E'_x = a_s e^{ik(\delta_s+\gamma)} + \sum_{n=1}^{N} \frac{1}{\sqrt{N}} a_p e^{ik\delta_n} \tag{12a}$$

y'-direction

$$E'_y = a_s e^{ik(\delta_s+\gamma)} - \sum_{n=1}^{N} \frac{1}{\sqrt{N}} a_p e^{ik\delta_n} \tag{12b}$$

The signal intensity at the x'-direction will then be

$$S'_x = a_s^2 + a_p^2 + \frac{a_p^2}{N}\left[\sum_{l=1}^{N-1} e^{ik\delta_l} \sum_{n=l+1}^{N} e^{ik\delta_n} + \sum_{l=1}^{N-1} e^{-ik\delta_l} \sum_{n=l+1}^{N} e^{ik\delta_n}\right] + \frac{a_s a_p}{N}\left[e^{ik(\delta_s+\gamma)} \sum_{n=1}^{N} e^{-ik\delta_n} + e^{-ik(\delta_s+\gamma)} \sum_{n=1}^{N} e^{ik\delta_n}\right] \tag{13}$$

and a similar expression can be obtained for S'_y. The third term in eqn. (13) represents the interference pattern due to the addition of speckles. The fourth term, which is of special interest to this study, represents the interaction of speckles with the reference beam.

Although speckles spatial frequencies vary over a wide range, only those frequencies that are concentrated about a mean value will interact with the reference beam. If the number of scatterers that produce the mean speckle frequency is L, the fourth term in eqn. (13) will become:

$$2a_s a_p \frac{L}{\sqrt{N}} \cos k(\delta + \gamma) \tag{14}$$

where $\delta = \delta_s - \delta$ is the mean phase. This result shows that the phase of the scattered light will carry information about the surface roughness, while the fringe visibility will decrease relative to specular surfaces. This conclusion is in accordance with previous observations about speckles,[19] and with our experimental results.

5 CONCLUSIONS

A diffuse point differential interferometer has been developed and used near the surface profile of camshafts. The interferometer was tested under laboratory conditions to evaluate its performance and the effects of speckles as well. The sensitivity of the interferometer was measured by comparing cold wire measurements of small temperature fluctuations in a shear layer against the interferometer signal. The interferometer is sensitive to optical pathlength variations in the order of 0·002 μm.

REFERENCES

1. Bennett, J. M. & Dancy, J. H. Stylus profiling instrument for measuring statistical properties of smooth optical surfaces. *Appl. Optics*, **20**(10) (1981) 1785.
2. Church, E. L., Vorburger, T. V. & Wyant, J. C. Direct comparison of mechanical and optical measurements of the finish of precision machined optical surfaces, *Opt. Eng.*, **24**(3) (1985) 388.
3. Bhusham, B., Wyant, J. C. & Koliopoulos, C. L. Measurement of surface topography of magnetic tapes by mirau interferometry, *Appl. Opt.*, **24**(10) (1985) 1489.
4. Jabr, S. N. Surface roughness measurement by digital processing of nomarski phase contrast images. *Opt. Lett.*, **10**(11) (1985) 526.
5. Rasigni, M., Rasigni, G. & Palmari, J. P. Study of surface roughness using a microdensitometer analysis of electron micrographs of surface replicas: I surface profiles, *J. Opts. Soc. Am.*, **71**(9) (1981) 1124.
6. Sommargren, G. E. Optical heterodyne profilometry, *Appl. Opt.*, **20**(4) (1981) 610.
7. Hockley, B. S. A computer controlled electro-optical dimensional gauging system used in manufacturing. *International Computer Technology Conference* ASME Century 2—Emerging Technology Conferences, San Francisco, August, 1980.
8. Doty, J. L., "Projection Moiré for Remote Contour Analysis", *J. Opts.*, Soc. Am., Vol. 73, No. 3 (1983).
9. Sawatari, T. Real-time noncontacting distance measurement using optical triangulation, *Appl. Opt.*, **15**(11) (1976) 2821.
10. Hatakoshi, G. & K. Goto, Grating lenses for the semiconductor laser wavelength, *Appl. Opt.*, **24**(24) (1985) 4307.
11. Asakura, T. & Erf, R. K. (eds), *Speckle Metrology*, Academic Press, New York, 1978.
12. Lorincz, E., Richter, P. & Engard, F. Interferometric statistical measurement of surface roughness. *Appl. Opt.*, **25**(16) (1986) 2778.
13. Smeets, G. & George, A. Instantaneous laser doppler velocimeter using a fast wavelength track michelson interferometer. *Rev. Sci. Instrum.*, **49**(11) (1978) 1589.
14. Smeets, G. A high sensitivity laser interferometer for transient phase objects. *Proc. of 8th International Shock Tube Symp.*, London, 1971.
15. Azzazy, M., Modarress, D. & Hoeft, T. High sensitivity boundry layer transition detector. *SPIE 29th International Symposium, No. 569 High Speed Photography, Videography, and Photonics III*, SPIE, Bellingham, Wash. (1985) 64

16. Swindell, W. Benchmark papers in *Optics*, Vol. 1, *Polarized Light*, Dowden Huchinsen and Ross, Pa. 1978.
17. Dainty, J. C. *Laser Speckle and Related Phenomena*, Springer-Verlag, New York, 1984.
18. Fujii, H. & Asakura, T. Effect of surface roughness on the statistical distribution of image speckle intensity, *Opt. Commun.*, **11** (1974) 35.
19. Francon, M., *Laser Speckle and Applications in Optics*, Academic Press, New York, 1979.